Moisture Adsorption in Palletised Corrugated Fibreboard Cartons under Shipping Conditions: A CFD Modelling Approach

T.M. Berry[1,2], A. Ambaw[2], T. Defraeye[4,5,6], C. Coetzee[1] and Umezuruike Linus Opara[2,3*]

[1]Department of Mechanical & Mechatronic Engineering, Stellenbosch University, Stellenbosch 7602, South Africa

[2]South African Research Chair in Postharvest Technology, Department of Horticultural Science, Stellenbosch University, Stellenbosch 7602, South Africa

[3]South African Research Chair in Postharvest Technology, Department of Food Science, Stellenbosch University, Stellenbosch 7602, South Africa

[4]Laboratory for Biomimetic Membranes and Textiles, Empa, Swiss Federal Laboratories for Materials Science and Technology, Lerchenfeldstrasse 5, 9014 St. Gallen, Switzerland

[5]Chair of Building Physics, ETH Zurich, Stefano-Franscini-Platz 5, 8093 Zürich, Switzerland

[6]Multiscale Studies in Building Physics, Empa, Swiss Federal Laboratories for Materials Science and Technology, Überlandstrasse 129, 8600 Dübendorf, Switzerland

*Corresponding author: Email: opara@sun.ac.za (U. L. Opara)

Highlights

- CFD model to predict moisture content in corrugated fibreboard developed
- Moisture dynamics in a refrigerated container during shipping
- Predicting changes in transient and spatial moisture content in cartons
- Ground work for future evaluation of carton mechanical strength

Abstract

Corrugated fibreboard packages (cartons) must support considerable mechanical loads during long term transport of fresh produce in refrigerated freight containers (RFCs). Fresh produce are transported under high relative humidity to reduce fruit moisture loss and preserve quality. However, these conditions can progressively reduce carton mechanical strength over time as a result of mechano-sorptive creep. Little is known regarding the actual moisture dynamics in stacked cartons in RFCs, which is important for mechanical strength assessments. To this end, a portion of a fully loaded RFC was investigated using a computational fluid dynamics (CFD) model, with respect to moisture transport in the air and the corrugated fibreboard. Simulations included the effects of loading, defrost cycles, fruit respiration and transpiration. Results

showed relatively low moisture content gradients in fibreboards through the stacked cartons under optimal shipping conditions. However, the initial activation of the RFC considerably accelerated the development of moisture content gradients in the cartons. Additionally, the most significant factor influencing spatial moisture gradients through the cartons was heat conduction from outside through the container wall.

Keywords: Corrugated fibreboard; Refrigerated shipping; Mechanical strength; Package design; Shipping conditions

1. Introduction

Ventilated corrugated fibreboard boxes (cartons) are used extensively (> 90%) to transport fresh produce from growers to consumers and play an essential role in fresh produce quality preservation (Berry et al., 2015). Corrugated fibreboard (CF or board) is generally preferred over other materials such as glass and plastic as it conveys several unique advantages. For example, (i) CF can be manufactured easily and sustainably from cellulose based products (e.g. wood and recycled plant materials) and is essentially made from paper, glued together with corn starch; (ii) CF is completely recyclable and biodegradable; (iii) CF is lightweight; (iv) CF has high rigidity for its density; and (v) CF has a dampening effect when fruit are exposed to mechanical loading such as impacts and vibration. However, an important challenge which influences ventilated carton design is to maintain carton mechanical strength under cold chain conditions over extended time periods (Pathare et al., 2012; Pathare and Opara, 2014; Fadiji et al., 2016; Fadiji et al., 2018). These conditions include high relative humidity environments and large compression forces, which have been largely unexplored in prior research.

During storage and shipping, compression forces occur as a result of pallet stacking, whereby cartons are palletised to form ~2 m high pallet stacks (pallet base/ footprint area ≈ 1.2 m^2) and cartons near the bottom of the stack must support the full pallet load (~1000 kg). High humidity conditions are necessary to minimise fruit moisture loss and preserve fruit quality. Fruit such as apples or citrus are, therefore, maintained between -0.5 and 5 °C at 90-95% relative humidity (RH) for periods between 4 and 6 weeks (Thompson et al., 2008), depending on the fruit type, market preference and export destination (Robertson, 2013). These high RH conditions result in large moisture contents (Parker et al., 2006) in the corrugated fibreboard, which adversely affect board strength, due to water molecules breaking hydrogen bonds in the cellulose fibre

(Allaoui et al., 2009). For instance, Pathare et al. (2016) observed a 47% reduction in carton compression strength after just two days storage at 90% RH.

High moisture content also influences the physico-mechanical properties of the corrugated fibreboard material (Parker et al., 2006; Sørensen and Hoffmann, 2003), which in turn can affect the mode of failure during compression. Previous work by the authors (Berry et al., 2017), examining the effect of vent hole design on carton strength, showed that certain vent hole designs were superior when matched to a particular board type (material properties). This has considerable implications on the assessment of new package designs since standard box compression tests are performed at 23 °C and 50% RH (TAPPI, 2012). However, in reality, the outcome of these evaluations may not be applicable to cold chain conditions. In order to address these concerns, more information is needed regarding the carton spatio-temporal moisture content distribution in the cold chain.

An equally important and often overlooked factor is the effect of creep. In this context, creep is defined as a relatively slow process, whereby a corrugated board material permanently deforms under the influence of mechanical stress (load). A subcategory of creep is mechano-sorptive creep, whereby the deformation process is significantly accelerated by varying humidity. Mechano-sorptive creep has been documented in both wood (Armstrong and Christensen, 1961; Armstrong and Kingston, 1960) and paper materials (Byrd, 1972a, 1972b), with many processes behind mechano-sorptive creep being proposed (Gibson, 1965; Haslach, 1994; Söremark and Fellers, 1993). However, subsequent studies suggest a process of nonlinear creep due to transient stresses from changes in board moisture contents (Alfthan, 2004, 2003; Alfthan et al., 2002; Habeger and Coffin, 2000). The resulting stresses (heterogeneous hygro-expansion and pallet weight) are, therefore, continuously redistributed and relaxed over time as the board deforms and moisture gradients change.

Mechano-sorptive creep is thus expected to play a significant role in the mechanical strength of cartons and their capacity to protect fresh produce against mechanical forces (compression, impacts and vibration). A common challenge reported in the fruit industry is the unexpected mechanical failure of one or more pallet stacks after an extended sea voyage in a refrigerated freight container (RFC). This is only discovered at the produce destination and is very costly due to the damaged fresh produce and investments for repacking. Curiously, in some cases, the RFC conditions over this period are reported to be normal. An improved understanding of the

conditions in RFCs leading to creep is, therefore, an important step towards improved horticultural carton designs and reduced postharvest losses. However, most studies have focused on mechanisms of creep in wood (Olsson et al., 2007) and paper (Haslach, 2000; Rahman et al., 2006). Little is known regarding transient moisture distribution and concentration in cartons during shipping, and specifically under hygrothermal conditions and mechanical loads which directly govern the rate and degree of creep.

Mathematical models could be very useful for studying moisture transport during shipping, as this helps to identify and explain the present challenges, and therefore to better design cartons and optimise performance evaluation methods. Numerical approaches, specifically computational fluid dynamics (CFD) have become a well-accepted approach to predict flow and scalar transfer processes in horticultural systems (Ambaw et al., 2013a; Delele et al., 2010; Norton et al., 2007; Zhao et al., 2016). This information could also be used to model moisture transport in cartons (Rahman et al., 2006) and to provide much greater insight with respect to carton strength and evaluation approaches. More informed decisions regarding carton design and the consequential reduction in both postharvest losses and material costs would be possible. To the best knowledge of the authors, a coupling of simulations of heat and mass transfer in the airflow to the hygrothermal transport in cartons has not been performed at this scale or for postharvest cold chain operations, such as RFC shipping.

The aim of this study was to develop a model to predict spatio-temporal moisture content distribution in corrugated fibreboard cartons under standard RFC shipping conditions. The proposed CFD model was validated under diffusion only and convection conditions, respectively. Using the validated model, the hygrothermal response of a portion of a RFC, loaded with packaged apple fruit, was simulated. The simulation incorporates a realistic airflow distribution as well as the effects of loading, defrost cycles, respiration and transpiration.

2. Materials and methods

The approach used in this paper with regards to materials and methods are outlined in Table 1.

This study applied two different validation experiments at separate scales. The small-scale experiment examined moisture sorption under diffusion only conditions inside a glass-chamber (section 2.4.1); whereas the larger-scale experiment examined moisture sorption under

122 convective conditions and was performed inside a CATTS chamber (Controlled
123 Atmosphere/Temperature Treatment System; section 2.4.2).

124 Experiments to determine initial and boundary conditions for the RFC simulation (section 2.5)
125 were determined by logging temperature and humidity conditions during commercial RFC
126 shipping voyages. Assumption and governing equations of the respective CFD model are
127 outlined in section 2.6. Finally, the geometries, computational domains and simulation setups
128 for the two validation simulations and the RFC simulation are described in section 2.7.

129 ## 2.1 **Fruit**

130 Apple fruit (cv. Golden Delicious) were purchased directly after harvest from a local grower in
131 the Western Cape (GPS), South Africa (March 2016). Fruit were free of visual defects, had an
132 average diameter of 62 mm (±8 mm; d), and were stored at -0.5 °C for a few days before
133 experiments were conducted. The thermal and material properties with respect to fruit density
134 (ρ), thermal conductivity (K) and specific heat (C_p) were taken as 845 kg m^{-3} (ρ_f), 0.427 W m^{-1}
135 K^{-1} (K_f) and 3 690 m^2 s^{-2} K^{-1} ($C_{p,f}$), respectively (Ramaswamy and Tung, 1981).

136 ## 2.2 **Corrugated fibreboard material**

137 ### 2.2.1 Corrugated fibreboard Properties

138 The corrugated fibreboard used throughout this study was supplied by APL Cartons (APL
139 Cartons (Pty) Ltd, Worcester, South Africa) and is commonly used to manufacture cartons for
140 fresh produce export. The CF was 4.2 mm thick (H), had a density of 167.5 kg m^{-3} (ρ_q), with
141 specifications of 250K/175C/250K (250 g m^{-2} Kraft Paper/175 g m^{-2} Tugela C-Flute/ 250 g m^{-2}
142 Kraft Paper) and an edge compression test value of 9.06 kN/m. The supplied CFs were
143 examined visually to ensure good condition and were stored at 20±1 °C and 50 ±5% RH before
144 the experiments.

145 ### 2.2.2 Samples and cartons used in glass and CATTS chamber experiments

146 Experiments performed in the glass-chamber made use of square CF samples, with dimension
147 of 9.0 × 9.0 cm, while maintaining equal volume and mass, respectively. A single-walled,
148 bottomless carton was manufactured (APL Cartons) for use in all CATTS chamber experiments

and is depicted in Figure 1a. The size of the cartons was reduced to 18% (of footprint area) of a standard apple carton, as used in the RFC simulations.

2.2.3 Carton design in RFC simulation

Specifications for cartons used in the RFC simulations represent a telescopic design (FEFCO and ESBO, 2007), which is formed from both an inner and outer carton (total wall thickness = 8.4 mm). The carton size and ventilation (area and positioning) were based on standard apple cartons used in South African exports (Mark 4; 500 × 333 × 270 mm), with total ventilation area (TVA) of 2.2% and 3.7% along the top/bottom and side walls, respectively (Berry et al., 2015).

2.3 **Measuring board moisture diffusion and sorption properties**

2.3.1 Board moisture diffusivity

A diffusion cup setup was used to estimate the effective moisture diffusivity (D_{eff}) through the CF (Figure 2). To achieve this, a constant moisture concentration gradient was maintained across a CF sample using saturated salt solutions. The diffusion cup was suspended inside an air-tight container (3 L) above a saturated salt solution (Potassium Nitrate; KNO_3; 94.6% RH), which provided a constant source of moisture to the chamber and experiments were performed at 20 °C and 1 °C (±0.1 °C), respectively. The inside of each diffusion cup was maintained at a lower moisture concentration by filling the inner volumes with a saturated solution of Sodium Chloride (NaCl; 75.5%). RH sensors (Tinytag TV- 4500, Hastings Data Loggers, Australia) were placed 5 mm above the CF board samples to determine the moisture concentration across the boards during the experimental period.

Circular CF samples were preconditioned at 84% RH for 3 days prior to the experiment and placed over the diffusion cup (Figure 2) to separate the chamber and inner cup regions with different moisture concentrations. A threaded ring was used to compress the board into rubber seals to ensure moisture transport was limited through the board region only. Fully assembled, the board sample exposed area (A_d; m^2) had a diameter of 55 mm. The experiment was performed in triplicate and ran over 24 days. The cup setup was weighed before and after each experiment to determine total moisture transport over the experimental period (G_d; kg s^{-1}). The D_{eff} value was then calculated using Eq. (1) (Radhakrishnan et al., 2000):

$$D_{eff} = G_d H / A_d \Delta c \quad (1)$$

where H is the board thickness (m) and Δc is the moisture content gradient across the board (kg m^{-3}).

2.3.2 Sorption isotherms

The equilibrium moisture content of the CF is influenced by the surrounding RH, and can be determined by a sorption isotherm (Parker et al., 2006). To characterise this relationship, board samples were equilibrated and measured for a range of RH conditions. Both dry and wet samples were examined since equilibrated moisture content values are higher during desorption (drying from high moisture content) than adsorption (hygroscopic loading from low moisture content). This phenomenon is commonly referred to as moisture hysteresis and is characteristic of the cellulose fibres in the CF (Chatterjee, 2001; Mualem, 1973; Peralta and Bangi, 1998). Moisture hysteresis can be defined as a time-based dependence of the moisture content in the CF, whereby the previous moisture content history of the board influences the current equilibrium moisture content (Chatterjee, 2001).

Dry samples were preconditioned by oven drying for 48 hours followed by storage at 0% RH (silica gel) until experiments commenced. Conversely, wet samples were preconditioned by soaking in a deionised water solution for 48 hours and were then stored at 100% RH (deionised water solution).The CF samples were then individually suspended at the centre of the sealed glass-chambers containing saturated salt solutions (at the bottom of the chamber) as detailed by Greenspan (1977), to create constant RH environments of 11, 36, 43, 67, 84, 95 and 100±0.1% around the samples. All experiments were repeated in triplicate at 1 and 20±1 °C, respectively, over a period of 72 hours. Moisture content (g/100$g_{dry\ fibre}$) was determined by weighing the sample on a balance (NewClassic MF: ML104/01, Mettler Toledo, Switzerland) immediately after the experiment and then taking the difference from the weight after oven-drying (100 °C, 48 hours).

2.4 **Model validation experiments**

2.4.1 Diffusion driven moisture sorption inside a glass-chamber

Validation experiments (performed in triplicate) measuring the rate of moisture adsorption and desorption in a CF sample were performed in glass-chambers (Figure 1b) under diffusion only conditions and compared to numerical simulation results. Samples were first oven-dried until the rate of mass change of the samples becomes zero (≈ 48 hours). Board samples were suspended in glass-chambers containing KNO_3 (94.6% RH) and weighed successively (every ~3.5 hours) over a period of 29 hours. Next, samples were relocated to new chambers containing K_2CO_3, which modified the glass-chamber RH to 43.2%. The relocation process took about 1-2 seconds and was performed at a RH of 50%. Very little effect from the environment was therefore expected. Samples were then again weighed successively over a period of 21 hours (every ~3.5 hours). Multiple glass-chamber/sample setups were run simultaneously (33 chambers in total), since the sample weighing process is disruptive to the experiment and each chamber can therefore only be measured once.

2.4.2 Convection-driven moisture sorption inside a CATTS-chamber

A second complimentary validation experiment investigating board moisture sorption and desorption was performed under forced convective conditions. Experiments were performed in a laboratory-scale CATTS (Controlled Atmosphere/Temperature Treatment System) chamber, manufactured by Techni-Systems (USA). To this end, corrugated fibreboard cartons were stored in a climate-controlled room (25 °C and 50% ±13% RH) for 48 hours prior to the experiments. Four cartons were placed centrally in the CATTS-chamber (Figure 1c). The CATTS-chamber is a flow through, airtight system with temperature and humidity control. The inlet to the chamber was fitted with a meshed plastic crate (external dimension of 57 × 38 × 40 cm with 60% open area), which supports the cartons in position to allow vertical flow of air. Air entered the chamber vertically from the bottom. The inlet air speed was measured (in triplicate) using 56 unidirectional velocity sensors (TVS-1100, Omega, USA). The air in the chamber is humidified by micro-misting nozzles. The conditioning regime inside the CATTS-chamber was pre-set on the device and the resulting conditions at the inlet, which changed gradually over time, were recorded using three temp/RH loggers (Tinytag TV- 4500).

At the start of the experiments, the temperature and RH inside the chamber was 25 °C and 59% RH (SD < 5%), respectively. Conditions in the chamber were then set to cycle between 35 °C at 98% and 22 °C at 30% RH. The conditioning cycles were as shown in Table 2. Conditions in the CATTS-chamber changed gradually to the set-point by the action of the heat/moisture sink or source. The conditions of the chamber were changed in such a way that the moisture concentration in the cartons never reached the EMC (i.e. the cartons were always in a state of adsorption/desorption). Additionally, at each of these periods (Table 2), one square sample (3 × 3 cm) was cut from each of the carton faces and immediately weighed, samples were then weighed again after being oven dried to determine moisture content. The resulting holes due to sampling were sealed with paper-based adhesive tape to maintain the carton's profile with respect to air distribution. Additional sampling between the adsorption and desorption cycles was not possible, as this would have vented the sealed chamber and irrevocably disturbed the conditions around the sample cartons.

2.5 **Determining conditions in refrigerated freight container during overseas transport**

Temperature inside a RFC packed with apple fruit was characterised over time to develop more realistic operating conditions boundary conditions for the CFD model. Three temperature loggers (LogTag Recorders Ltd., Auckland, New Zealand) were thus placed in the bottom, middle and top cartons of a single apple fruit pallet stack. With respect to the horizontal plane, loggers were positioned inside cartons, at the centre of the stack. Loggers were added during the container loading process (August 2015) and the respective pallet stack was situated near the RFC door. The container was then transported via truck from a Grabouw pack house to the Cape Town docks (70 km; South Africa) and then shipped to the United Kingdom (UK) over a period of 18-days. Temperature and RH data from subsequent RFC exports (4 shipments) was used to confirm the initial temperature data's validity. In addition, the four shipments were also used to determine general moisture concentration profiles over the shipping durations.

2.6 **Numerical model**

2.6.1 Model Concept and Assumptions

A mathematical model describing moisture adsorption, desorption and diffusion through fibreboard sheets (Radhakrishnan et al., 2000; Bandyopadhyay et al., 2002, 2000) was applied in this study for the purpose of predicting moisture transport through corrugated fibreboard

under RFC conditions. The model was extended by including convection terms to the moisture diffusion-adsorption process, as well as including the presence of cartons packed with loose fruit.

In addition to the final RFC simulation, two separate validation simulations were performed to test the model's ability to predict board moisture transport. The first validation simulation (section 2.4.1) predicted moisture sorption in a board sample, inside an air-filled glass chamber under diffusion only conditions. The second validation simulation (section 2.4.2) predicted moisture sorption in several small, empty cartons inside a CATTS-chamber under convection airflow conditions. Finally, the RFC simulation applied the model to predict moisture sorption in a portion of a pallet stack comprised of explicitly modelled cartons, packed with apple fruit under realistic (ideal temperature and airflow rates) RFC conditions. The numerical model applied in the RFC simulation are detailed below. Since the glass-chamber and the CATTS-chamber were relatively simple, it was possible to develop a detailed CFD model that consider all geometric descriptions of the system: the fruit and the package box designs, which is more realistic. This is in direct contrast to fruit loaded reefer containers or cool store rooms, where porous medium approximation is mandatory to apply CFD (Ambaw et al., 2014).

The assumptions made in this numerical study should be acknowledged in order to fully appreciate its contribution to the existing knowledge on moisture transport in fibreboard materials, and to identify developments and refinements that could be applied in future models. The Corrugated fibreboard material (all simulations) was assumed to be a composite solid material with spatially uniform air-to-fibre ratio. Material properties (density, thermal and moisture diffusion properties) were assumed uniform and estimated based on the air-to-fibre ratio. Moisture transport in the air zones was described using a passive scalar transport equation, since the moisture content in the air is very dilute (< 1%) and thus has an almost negligible effect on the air properties.

Spherical fruit in the RFC simulation were assumed to be homogenous with constant material properties throughout. The volume inside the cartons consisting of loose fruit (solid) and air (fluid) and was treated as a porous domain. The two phases in these volumes therefore formed a continuum and interfaces were not resolved geometrically, but are instead parameterized through the volume averaging procedure (Hassanizadeh and Gray, 1979). The airflow resistance of the porous medium was described using an isotropic loss model with linear

coefficients, which were previously determined in a dedicated wind tunnel experiment (material and methods described by Ngcobo et al. (2012)). Although not as accurate as an explicitly modelling the fruit, the porous media approach still produces satisfactory results (Ambaw et al., 2013b), while significantly reducing computational costs. This approach is valid, as the primary intent in this study was to include the thermal capacity of the fruit into the model and not to perfectly imitate a specific case setup, but rather to investigate a generic case example.

2.6.2 Governing equations

Reynolds-averaged Navier Stokes (RANS) equations were used to solve airflow, energy and scalar (moisture) transport in the air with the shear stress transport (SST) k–ω turbulence model (Menter, 1994). This particular turbulence model performs best compared to other turbulence models in postharvest cooling of spherical produce in similar cases and has been validated extensively in previous work by the authors (Ambaw et al., 2014, 2013b, Delele et al., 2012, 2009; Hoang et al., 2015). This study builds on previous work (Ambaw et al., 2017, 2014, 2013c, 2013b), which have detailed many of the governing equations, assumptions and validations used for CFD of horticultural packaging simulations. The section below thus mainly address how the moisture transport and porous media components of the model were included.

For the porous domain (packed fruit inside cartons for the RFC simulation), the moisture transport was described by Eq. (2) and (3) (Chourasia and Goswami, 2007).

$$\varepsilon_a \frac{\partial c_a}{\partial t} + \varepsilon_a \frac{\partial}{\partial x_i}\left(u_i c_a\right) = \frac{\partial}{\partial x_i}\left(D_a \frac{\partial c_a}{\partial x_i}\right) + S_c \tag{2}$$

$$S_c = -\frac{\partial c_f}{\partial t} = k_m A_f \left(c_f - c_a\right) \tag{3}$$

where ε_a is the porosity inside the cartons (0.57), c_a (kg m^{-3}) is the moisture content in the air zone, A_f is the specific area of the fruit in the air zone (63.8 m^2 m^{-3}), c_f (kg m^{-3}) is the fruit moisture content and S_c (kg m^{-3} s^{-1}) is the moisture loss as a result of transpiration.

Transpiration from fruit was treated as a constant source of moisture at the air-fruit interface. Fruit flesh is saturated with moisture containing various dissolved minerals and sugars,

316 resulting in a vapour pressure lowering effect, where the intercellular moisture concentration
317 (c_f) is slightly below saturation (c_{sat}). The resultant saturation moisture content of apple fruit
318 (c_f) was determined to be 98% of the c_{sat} value (Chau et al., 1987). k_m (m s^{-1}) is the effective
319 interfacial moisture transfer coefficient and is determined from properties of the air layer over
320 fruit surface and skin of the fruit as: $k_m = (1/k_a + 1/k_f)^{-1}$, where k_a, and k_f are the resistance of
321 the air film and the fruit skin to moisture transfer, respectively. The corresponding k_f value was
322 obtained (1.06×10^{-4} m s^{-1}) from Kessler and Stoll (1953) and k_a was determined from the
323 Sherwood number, which was calculated using the Sherwood-Reynolds-Schmidt correlation
324 (Becker et al., 1996; Chau et al., 1987; Geankoplis, 1978) as shown in Eq. (4).

$$Sh = \frac{k_a d}{D_a} = 2.0 + 0.552\,\mathrm{Re}^{0.53}\,Sc^{0.33} \tag{4}$$

325 Where Re is the Reynolds number ($(\rho_a v d)/\mu_a$), ρ_a is the air density (kg m^{-3}), v is the air velocity
326 (m s^{-1}), D_a is the moisture diffusivity in the air, μ_a is the air dynamic viscosity (Pa s) and Sc is
327 the Schmidt number ($\mu_a/(\rho_a D_a)$).

328 Two phase volume-averaged equations (Eq. (5) and (6)) were used to model the heat transfer
329 inside the porous domain (Smale et al., 2006; Zhao et al., 2016):

$$\varepsilon_a \rho_a C_{p.a} \frac{\partial T_a}{\partial t} + \varepsilon_a \rho_a C_{p.a} \frac{\partial}{\partial x_i}\left(u_i T_a\right) = \frac{\partial}{\partial x_i}\left(K_a \frac{\partial T_a}{\partial x_i}\right) + h_{conv} A_f \left(T_f - T_a\right) \tag{5}$$

$$\left(1-\varepsilon_a\right)\rho_f C_{p.f} \frac{\partial T_f}{\partial t} = \frac{\partial}{\partial x_i}\left(K_f \frac{\partial T_f}{\partial x_i}\right) + h_{fs} A_f \left(T_a - T_f\right) + S_e \tag{6}$$

330 where $C_{p,a}$ (J kg^{-1} K^{-1}) is the air heat capacity at constant pressure, K_a (W m^{-1} K^{-1}) is the
331 effective thermal conductivity in the air, T_a (K) is the air temperature, T_f (K) is the fruit
332 temperature and u (m s^{-1}) is the air velocity.

333 Thermal coupling between the fluid and solid phases in the porous domain as a result of
334 convective heat transfer was characterised as a function of the heat transfer coefficient h_{fs} and
335 the specific area (A_f). For the RFC, the Biot number (Bi) was determined to be about 0.6 on
336 average, but higher near vent holes where flow accelerated. The internal thermal resistance of

337 the apple flesh was therefore included in the model. Under the respective conditions and for
338 spherical apple fruit, the average fruit temperature is situated at ¾ of the apple radius (van der
339 Sman, 2003). The h_{fs} was thus calculated using Eq. (7).

$$h_{fs} = \left(\frac{1}{h_{conv}} + \frac{d}{8K_f} \right)^{-1} \quad (7)$$

340 The corresponding heat transfer coefficient (h_{conv}; W m^{-2} K^{-1}) was calculated using Eq. (8),
341 which is the Nusselt-Reynolds-Prandtl ($Pr = (\mu_a C_{p,a})/(\rho_a K_a)$) correlation (Becker et al., 1996).
342 This is similar in form to Eq. (4), except the Sherwood and Schmidt numbers are replaced with
343 the Nusselt and Prandtl numbers, respectively:

$$Nu = \frac{h_{conv} d}{K_a} = 2.0 + 0.552\,\mathrm{Re}^{0.53}\,\mathrm{Pr}^{0.33} \quad (8)$$

344 The heat source term (S_e) in the fruit region of the porous medium (Eq. (6)) was determined as
345 the sum heat loss from transpiration ($Q_{lat} = L_s S_c$; W m^{-3}) and the respiration heat (Q_{resp})
346 generated by the apple fruit ($S_e = Q_{resp} + Q_{lat}$). The latent heat of evaporation (L_s = 2499.1 J
347 kg^{-1}) was determined at 0.8 °C as the average temperature during shipping (ASHRAE, 2009).
348 Respiration heat was calculated from Eq. (9) as taken from USDA (1986) and Becker et al.
349 (1996) for apples:

$$Q_{resp} = \left(1 - \varepsilon_f\right) \rho_f \left(2.778 \times 10^{-3} \left(f \left(1.8 T_f + 32 \right)^g \right) \right) \quad (9)$$

350 where the f and g coefficients are determined from USDA (1986) to be 5.5671 × 10^{-4} and
351 2.5977, respectively; ρ_f is the apple fruit density and T_f (°C) is the fruit temperature.

352 The corrugated fibreboard was modelled as a solid domain with two concentration fields. One
353 for the moisture concentration within the void (c_p; i.e. air gaps between the corrugations and
354 the air-filled inter-fibre regions) and one for the moisture content in the fibres (c_q; fibreboard).
355 The model expressed board moisture contents as a concentration value (c; kg m^{-3}), however,
356 this value can also be expressed as a weighted average (g/100g$_{\text{dry fibre}}$): $q = 100 c_q / \rho_q$. The model

for moisture transport in the two regions for the board is given by Eqs. (10), (11) and (12) (Bandyopadhyay et al., 2002, 2000):

$$\frac{dc_p}{dt} = -D_{eff.p}\nabla^2 c_p - r_s \tag{10}$$

$$\frac{dc_q}{dt} = -D_{eff.q}\nabla^2 c_q + r_s \tag{11}$$

$$r_s = k_i\left(c_x - c_q\right) \tag{12}$$

where r_s accounts the adsorption and desorption of moisture inside the corrugated fibreboard (Eq. (12)), k_i is the intra-fibre mass-transfer coefficient or a local moisture exchange coefficient (0.0035 s^{-1}) as determined by Bandyopadhyay et al. (2002, 2000) and c_q is the moisture content in the fibres of the board.

The c_x in Eq. (12) is the equilibrium moisture content (EMC) in the fibres of the board (kg m^{-3}) as determined by the Peleg four-parameter model (Eq. (13) and (14)). At high RH conditions (> 95%), it was found that the Peleg model better fit the moisture sorption isotherms than the commonly used Guggenheim–Anderson–deBoer model (Basu et al., 2006; Labuza and Altunakar, 2007; Peleg, 1993).

$$c_x = \frac{q_x \rho_q}{100} \tag{13}$$

$$q_x = Aa_w^B + Ca_w^D \tag{14}$$

where A,B,C and D are dimensionless coefficients, q_x (g/100$g_{dry\ fibre}$) is the weighted average value for the EMC an a_w is water activity (-).

2.7 **Geometry and computational domains**

Geometries corresponding to the three models are shown in Figure 1b, Figure 1c and Figure 3b. The computational mesh was a hybrid grid (tetrahedral and hexahedral cells). The spatial

discretisation error was evaluated by means of a grid sensitivity analysis together with a generalised Richardson extrapolation (Celik et al., 2008; Roache, 1994). The grid size used in the pallet stack simulation was 1 002 267 cells, where the average discretisation error in estimated moisture content in board was 1%.

2.7.1 Boundary and initial conditions

The computational domain corresponding to the glass-chamber validation experiment consists of the board region (solid domain) as submerged in the free air region (fluid domain). The surface of the board sample was set as a no-slip wall to airflow and a conservative flux for moisture transfer (c_p). The glass wall was modelled as no-slip adiabatic wall. The bottom boundary (Figure 1b), which represented the saturated salt solution, was set as a no-slip adiabatic wall with a fixed additional moisture value equal to 95% and 43% RH (16.2 g m^{-3} and 8.1 g m^{-3}) for 29 hours and then 20 hours, respectively.

Similar to the glass-chamber case, the computational domain for the CATTS experiment consists of the carton region (board material, solid domain) and a free air region (fluid domain). The computational domain was reduced by imposing a symmetry plane (slip walls) vertically through the domains (Figure 1c), which assumed normal velocity components and normal gradients at the boundary are zero. The surface of the cartons was set as a no-slip wall for airflow and a flux boundary condition was applied for heat and moisture transfer. The walls of the chamber were modelled as no-slip adiabatic walls. Zero static pressure was imposed at the outlet boundary and the inlet boundary was set according to the velocity profile as determined in section 2.4.2. Furthermore, the temperature and moisture content values at the velocity inlet boundary were set to match the experimental conditions as reported in section 3.2.2.

Figure 3b shows the model geometry for the RFC pallet stack case, which represents a portion of a fully packed RFC (Figure 3a). Similar to the validation cases, the cartons are explicitly accounted. The geometry of the individual cartons is shown in Figure 3c and are each packed (loose) with 21.6 kg of ‘Golden Delicious’ apple fruit. The apple-fruit regions were modelled as a porous medium domain and the pallet base region under the cartons was modelled as an air domain. A symmetry plane was imposed half way through the pallet stack to reduce computational grid size and thus simulation time. The surface of the cartons was set as a no-slip wall to airflow and a conservative flux for heat and moisture transfer. A pressure profile

406 was imposed at the pressure openings (Figure 3a) to generate a realistic flow field in the pallet
407 stack, which was attained from a validated full scale simulation of a RFC packed with fruit
408 (Getahun, 2016). Temperature and moisture conditions at the pressure openings were
409 determined from experimental results, as discussed in section 3.3.1. Heat entering the RFC
410 from the outside of the container (T_O; temperature varied with time) was included along the
411 pallet boundary wall exposed to the RFC side. The sensible heat gain ($q_{r,w}$; W) through the wall
412 was calculated as Eq. (15) and the corresponding overall coefficient of heat transfer (U_w) of the
413 RFC wall was estimated using Eq. (16) as determined from ASHRAE (2006). For this study,
414 the U_w was determined to be 0.13 W m^{-2} K^{-1}.

$$q_{r,w} = U_w A_w \Delta T \tag{15}$$

$$U_w = \frac{1}{h_{i,w} + x_w / k_w + h_{o,w}} \tag{16}$$

415 where A_w is the RFC wall area (m^2), ΔT (K) is the temperature difference between the outside
416 and inside of the RFC wall, $h_{i,w}$ is the inside surface conductance (1.6 W m^{-2} K^{-1}; (ASHRAE,
417 2006)) for the trapped pockets of air between the pallet stack and the RFC wall, x_w is the RFC
418 wall thickness (0.15 m), k_w is the thermal conductivity of the RFC wall (polyurethane; 0.022
419 W m^{-1} K^{-1}; (ASHRAE, 2006)) and $h_{o,w}$ is the outside surface conductance (6 W m^{-2} K^{-1};
420 (ASHRAE, 2006)), which assumes the outer RFC wall was exposed to an average wind speed
421 of 25 km h^{-1} over the shipping duration.

422 2.7.2 Simulation setup

423 Simulations were performed using Ansys-CFX 16.2 CFD (Ansys Inc., Canonsburg, PA, USA)
424 code, which uses the finite volume method. The simulations used second order backward Euler,
425 high resolution spatial differencing (i.e. a blend between central differencing and upwind
426 differencing locally) and second order schemes for the transient, advection and turbulent term.
427 Before performing transient moisture and heat simulations, the initial flow field conditions was
428 determined using steady-state simulations (CATTS and Pallet stack). The flow field was then
429 disabled during transient simulations, which reduced computational cost as only the scalar and
430 energy equations were solved. Several time step sizes (90, 45, 15, 10, 5, 1 s) were examined
431 for sensitivity and were assessed with respect to accuracy, convergence history and computing

time. A time step of 15 s with 25 iterations was selected as optimal and showed good predictions compared to experimental results. The pallet stack simulation took about 35 days using 24 cores on a high-performance computing cluster (Rhasatsha).

3. Results and discussion

3.1 Board properties

3.1.1 Fibreboard diffusivity

Table 2 summarises the moisture diffusivity and physical properties of the board and its respective components. The total effective moisture diffusivity (D_{eff}) was calculated using Eq. (1), with the moisture gradient (Δc) between the inner and outer RH values in the experimental cup setup (Figure 2). The inner RH at the board surface was taken to be equal to the NaCl solution (75.5% RH), since the air gap (< 5 mm) has a much higher diffusivity compared to the CF sample (Radhakrishnan et al., 2000). The outer surface had an average RH of about 88% ±4% (at both 20 °C and 1 °C), as determined by the data loggers.

Moisture transport occurs through two regions in corrugated fibreboard, namely, through the cellulose fibres ($D_{eff,q}$) and air components ($D_{eff,p}$). Two air regions are present in CF, namely, inter-fibre air regions (D_p; Table 2) and the large air gaps between the CF fluting/liners (D_a; Table 2). According to Bronlund et al. (2014), $D_{eff,p}$ can be estimated from the sum of these total resistances and their respective thicknesses (fibreboard = H_p; air = H_a) using Eq. (17).

$$D_{eff.p} = \frac{H}{\left(\frac{H_p}{D_p} + \frac{H_a}{D_a}\right)} \tag{17}$$

Moisture diffusion through the fibre component of the CF ($D_{eff.q}$) occurs in parallel to the $D_{eff.p}$ (air components) and can therefore be estimated as: $D_{eff} = D_{eff.p} + D_{eff.q}$ (Table 2). For corrugated fibreboard, Bronlund et al. (2014) showed that diffusion through the fibre component is less critical to moisture transport than in non-corrugated fibreboard (thicker paperboard). This is due to the fluted geometry in the board, which considerably slows diffusion as a result of the tortuous path.

456 It should be noted that diffusivity of moisture in corrugated fibreboard is a somewhat complex
457 mechanism, as the rate of transport is dependent on the direction of travel, due to the non-
458 uniform geometry. However, lateral moisture transport along the length of the board is
459 considered less critical under the conditions examined in this study. This is due to local
460 differences in board moisture content being quite low, as a result of the relatively small air
461 moisture gradients across the board surfaces. The moisture diffusion rate normal to the board
462 surface was thus used uniformly in this study.

463 3.1.2 Board moisture content

464 The adsorption and desorption curves with respect to water activity are shown in Figure 4. The
465 adsorption curves were obtained by hygroscopically loading samples from a dry state and the
466 desorption curves were obtained by drying samples from a wet state. This was done to fully
467 capture the maximum desorption and minimum adsorption curves, which differ as a result of
468 the moisture hysteresis phenomenon. Specifically, board EMC values are higher during
469 desorption than adsorption and depending on the moisture history and will always lie within
470 the maximum and minimum curves (Figure 4) (Chatterjee et al., 1997).

471 The resulting curves (Figure 4) were mainly linear, with an upward concave trend when
472 $a_w > 0.9$. Each respective curve was characterised using the Peleg (Eq.(14); $R^2 > 0.99$) model
473 (Labuza and Altunakar, 2007; Marcondes, 1996), for which the resulting coefficients are also
474 reported in Figure 4. In addition, the Peleg model was fitted to the combined data, to generate
475 average moisture sorption isotherm curves. Interestingly, the difference between the adsorption
476 and desorption curves at 20 ºC (Figure 4a) was relatively small compared to 1 ºC (Figure 4b).
477 This can be attributed to the additional available heat energy, which better enables water
478 desorption from the cellulose fibres (Cleland et al., 2008).

479 Figure 4a and b emphasises the phenomenon that the sorption isotherms often vary slightly at
480 different temperatures (Parker et al., 2006). According to Sørensen and Hoffmann (2003) these
481 differences can range from 3% to 4% (2-25 °C), which is consistent with the findings from
482 earlier studies (Darling and Belding, 1946; Skogman and Scheie, 1969; Wahba and Nashed,
483 1957). In this work, the 20 ºC and 1 ºC adsorption curves had relatively similar (~5%) EMC
484 values for $a_w < 0.90$, whereas at $a_w > 0.90$, the 1 ºC EMC values were about 20% lower than

485 the 20 ºC curve. Conversely, the desorption curves differed substantially, with 33% and 50%
486 larger EMC values for $a_w < 0.90$ and $a_w > 0.90$, respectively.

487 RFCs and cold rooms typically function within relatively narrow RH ranges (90-95% RH;
488 section 3.3.1). Moisture hysteresis is, therefore, not expected to have a critical effect on EMC
489 (q_x) values inside the RFC. Hysteresis was, therefore, not included within the scope of this
490 study and the average of the two curves (Figure 4b) was used in the RFC CFD model.

491 ## 3.2 **Model validation**

492 The CFD model was validated using experiments at two separate scales (Table 1). At small
493 scale, moisture diffusion adsorption/desorption dynamics were examined in a single CF
494 sample, which was suspended in a sealed glass-chamber. Next, at medium scale, the
495 convection-diffusion adsorption-desorption dynamics of moisture transport of the model is
496 validated in a CATTS-chamber packed with four cartons.

497 ### 3.2.1 Glass-chamber validation

498 Figure 5 compares predicted and measured moisture content values versus time for an
499 adsorption process followed by a desorption process inside a glass-chamber holding a CF
500 sample (at two temperatures). There was good agreement between predicted and measured
501 values. A discrepancy between the model and experimental results was observed at the end of
502 the desorption curves, particularly at 1 ºC. A contributor to this may be attributed to hysteresis,
503 whereby the moisture content history in the board influences the EMC value. Specifically, the
504 adsorption/desorption curves (Figure 4) were quite similar at 20 ºC, but differed somewhat at
505 1 ºC. However, since RFCs operates in relatively small RH ranges (85-95%), hysteresis was
506 not considered in model development, as it would have a near negligible effect on predictions.
507 It should be noted for future studies, however, that previous studies have proposed some
508 approaches to integrate the adsorption and desorption curves towards predicting hysteresis
509 loops (Chatterjee, 2001; Chatterjee et al., 1997). Overall, the glass-chamber validation study
510 demonstrated the model's capacity to accurately predict moisture transport between the air and
511 board domains.

3.2.2 CATTS-chamber validation

Figure 6a shows the temperature and RH treatment protocol applied in the CATTS-chamber. The resulting volume-averaged moisture content in the cartons is further shown in Figure 6b, as determined from experimental measurements and CFD predictions. Based on the similar moisture adsorption and desorption trends and values, acceptable agreement between the experimental and predicted values was observed, indicating good predictive power by the model. Some variability was observed in the first experimental readings (7.9 hours), which can be ascribed to slight differences in initial carton moisture contents before each experiment. The EMC value (g/100$g_{dry\ fibre}$), as calculated from the RH (Figure 6a) in the chamber and the PELEG equation (Eq. (14)); Figure 4) are shown in Figure 6b. The difference between the plotted EMC and the moisture content thus demonstrates the cartons were always in a state of sorption/desorption throughout the experiment (i.e. never at equilibrium). The CFD model thus demonstrated its capacity to realistically simulated moisture transport in CF during convective airflow, under relatively complex conditioning treatments.

Figure 7a shows the predicted flow field along the symmetry plane of the CATTS-chamber. The CATTS inlet has a higher air velocity along the left side (door), which was characterised in the model using an experimentally determined velocity profile (average velocity of 5.9 m s^{-1}). For the bottom portion of the chamber (volume near the cartons), the CFD simulations showed a volume-averaged velocity of 6.6 m s^{-1} and a Reynolds number of 1.9×10^5. Flow in the CATTS-chamber was thus turbulent, which consequently minimised moisture gradients in the chamber and across the carton surfaces (standard deviation of 0.5% RH).

The moisture gradients present in the cartons were mainly a factor of the convective mass transfer coefficient (CMTC) and board thickness. The walls parallel to the symmetry plane were the location of highest moisture heterogeneity (2-5% different to carton average), due to the additional thickness (two boards) and the low CMTC (1.39×10^{-2} m s^{-1}), where the average CMTC along the carton surfaces was 2.28×10^{-2} m s^{-1}.

3.3 **Moisture distribution inside refrigerated freight containers**

3.3.1 Conditions in pallet stack for model setup

Figure 8a shows the experimental air temperature logger data as recorded at the bottom of the pallet stack during shipping from South Africa to the UK. The results showed an uneventful voyage, with ideal temperature regulation throughout the shipping duration and was consistent with temperature profiles in subsequent export journeys. The initial temperature conditions inside the RFC simulation were consequently set uniformly across the pallet domains as 0.8 °C, as per the recorded values.

RH profiles from RFC export journeys showed values remained at about 90% ±3% RH, while fluctuations were mainly attributed to changes in temperature. In contrast, moisture concentration values (kg m^{-3}) was relatively consistent and generally ranged by about 2.9×10^{-4} kg m^{-3} per day, which is equivalent to about 5% RH (at 1 °C). This small variation can be attributed to the closed environment of the RFC, whereby changes in moisture concentration are mainly a function of condensation on the evaporative coils (refrigeration unit) and transpiration from the packed fruit.

Analysis of the results showed three prominent contributors to temperature variability. The initial large peak in temperature ($T_{P;}$ Figure 8) on the 1st day was due to the container refrigeration unit and fan system being activated on the vessel after an extended period without power. Heat that had collected in the air near the RFC's walls was thus first gradually forced up into the pallet stacks and then over time (about 6 hours) replaced with cool refrigerated airflow. Short (45 minutes) temperature peaks occurred daily and are a result of defrost cycles ($T_{D;}$ Figure 8a), whereby the refrigeration unit's evaporation coils are heated to eliminate ice build-up (ASHRAE, 2000). Finally, the main bell shaped temperature curve ($T_{M;}$ Figure 8a) over the whole shipping duration is attributed to the outside temperatures ($T_{O;}$ Figure 8a), which were lowest at the start (South Africa) and end (UK), and highest half way through the journey (Earth's equator). It was possible to estimate the T_O (outside temperature) using sea surface temperature (SST) data from NASA JPL (Jet Propulsion Laboratory) ROMS (Regional Ocean Modelling System) group (Figure 9), which ranged between 13 °C and 27 °C over the 18-day period. Correlating T_M and T_O, showed that T_O can be expressed in terms of T_M: $T_O = T_M \times 23 + 4$ °C ($R^2 = 0.94$).

Given the complexity of the RFC simulation and the large computational time required (~5 days run time for each simulation day) it was necessary to condense the conditions over the 18-day voyage into a 7-day simulation period (Figure 8b). Specifically, the T_M curve was scaled (with respect to the time domain), the T_P peak was left unchanged (~1 day) and the daily occurrence period, range and domain of the individual T_D defrost cycles were kept constant. The simulation thus provides insight into cartons responses to the various RFC conditions. Although, it is expected that the simulations final state will differ somewhat to reality as a result of the condensed timeline.

The temperature and moisture content of air entering the simulated pallet at the pressure openings (Figure 3b) was set uniformly, as indicated in Figure 8a, whereas the outside temperature was set to T_O. Moisture concentration in the RFC simulations was thus initialised as 4.9×10^{-3} kg m^{-3} in the air domains (c_a) and inter-fibre air (c_p) regions and 27.2 g/100$_{\text{dry fibre}}$ in the fibre regions (c_q) of the carton domains. The airflow distribution along the middle of the domain (parallel to the RFC length) is shown in Figure 7b. The volume-averaged air speed in the cartons and pallet base regions was 0.02 m s^{-1} and 0.63 m s^{-1}, respectively. Figure 7b shows that inside the cartons, air flowed in a mainly diagonal direction (up and left = towards the RFC doors; Figure 3b). With respect to the pallet base, air was flowing mainly from the right side of the pallet base and up the T-bar floor to the left side of the pallet base, with a small portion entering the cartons.

3.3.2 Carton moisture content over the shipping duration

Conditions in the RFC represent an ideal shipping journey, without any cold chain breaks or equipment failures. The resulting CF moisture content values and distributions are therefore typical of desirable shipping conditions and provides a valuable baseline against which future studies incorporating cold chain breaks can be compared. The volume-averaged temperature and relative humidity in the cartons and air/fruit (porous) regions are shown in Figure 10a and b. The temperature in the carton region generally followed a similar trend to the air temperature profile (0.8-1.8 °C). A slightly larger (0.2 °C) average temperature was predicted in the cartons compared to the air region, due to the heat conduction into the cartons from the RFC wall. Furthermore, the three temperature features (T_P, T_D, T_M) were observable in the cartons but were attenuated compared to the inlet conditions (Figure 8b).

As expected, the range of RH conditions in the stacked cartons were rather small, which is a desirable goal during RFC shipping. The RH curve in the cartons had a more linear profile than in the air region (Figure 10b). The RH in the porous region is mainly a function of the inlet temperature and moisture concentration. Specifically, RH values in the porous region ranged between 91.8% and 94.7% RH (Δ2.8%), whereas the carton inter-fibre (air) region ranged between 92.8% and 93.0% RH (Δ0.2%). The relative uniformity in the carton RH can be attributed to the fibreboard acting as a buffer to changes in RH. Fibreboard has a large moisture content capacity (~8000 times more than air per a volume) and its equilibrium value (q_x) is a function of the RH in the board (Eq.(14)). Consequently, an increase or decrease in board a_w results in a rapid decrease or increase in air moisture concentration, respectively, as moisture is transported between the air (inter-fibre) and fibres. Conditions inside the cartons were therefore more influenced by the long-term T_P and T_M curves, than by the smaller defrost cycles (T_D). The impact of defrost cycles on mechano-sorptive creep has been a topic of speculation in the fresh produce industry, however, these findings suggest it to be a minor contributor under these circumstances.

Figure 10c shows the average moisture content in the cartons over the shipping duration. As expected, the trend of the board moisture content was a function of the difference in RH between the carton and air regions (Figure 10b). The initial moisture content value was set at 27.2 g/100$g_{\text{dry fibre}}$ (equivalent to 276 g H_20 per a carton), based on the initial temperature and air moisture conditions. However, the heat gain from the RFC wall lowered the overall RH and thus the equilibrium moisture content. A generally negative moisture content trend was consequently observed, with volume-averaged values ranging between 26.9 g/100$g_{\text{dry fibre}}$ and 27.3 g/100$g_{\text{dry fibre}}$. This is expected to be a relatively realistic scenario, since pallet stacks are first stored as high RH conditions (90-95% RH) before being loaded into the RFC. Setting initial board moisture content values close to the ECM made it possible to detect the realistic effects of the loading temperature peak (T_P) and general equatorial temperature trend (T_M).

3.3.3 Moisture content gradients in cartons

Figure 11 show the distribution of moisture in the stacked cartons at one-day intervals. A uniform board moisture content value was initially set across the stacked cartons (Day 0), which then gradually developed over the simulated duration. The development of a moisture content gradient across the stacked cartons between the RFC wall and opposite pallet side is

visible. The evolution in moisture content distribution in the stacked cartons between day 1 and day 7 suggests the distribution may further develop if a longer shipping duration is used. The transient change in moisture content inside a RFC is therefore a long-term process and could potentially last several weeks.

Figure 12 depicts the board moisture content values along vertical lines throughout the stacked cartons after 7-days. The graph shows a generally even board moisture content gradient through the stack. Variations can be attributed to different board volume-to-surface-area ratios. For instance, larger moisture content values (peaks) occurred near the carton corners and edges. The board moisture content distributions in the stack were mainly a function of differences in RH, which in this study were relatively small. Total moisture transpiration at the examined shipping temperature (1.5 °C for fruit) was about 500 g over the 7-days (0.22% of fruit mass) and therefore did not have a large influence on moisture RH gradients between the individual cartons. However, potentially larger effects are expected across an entire RFC, at higher temperatures (cold chain breaks, larger transpiration rates) or when using fruit with higher transpiration rates (e.g. stone fruit). Similarly, respiration heat (6 W across examined domain) did not significant influence airflow temperature within the stack.

Figure 13b shows that moisture content gradients in the stacked cartons corresponded closely to the temperature gradient. In this case, temperature was the most significant factor driving changes in moisture content across the pallet stack. This is due to the dependence of the board EMC (q_x) on water activity, which is a factor of temperature. It should be noted that the pallet stack in this study were assumed to be an equal distance from the RFC wall, resulting in a constant rate of heat conduction into the stacked cartons. Although this is often the case, slight differences in pallet loading can also result in varying gaps and contact areas with the RFC walls.

Temperatures in RFCs can also vary in reality, depending on the time of year and quality of the RFC, whereas breaks in the cold chain can result in more substantial temperature and RH variations. For example, when refrigeration is halted (power break); large temperature differences between pallet stacks due to inadequate forced-air cooling (Brosnan and Sun, 2001); ambient loading, whereby pallet stacks are loaded warm and cooled over the shipping duration (Defraeye et al., 2015); and intermittent warming treatments, where the packed fruit

659 are continuously heated and cooled during shipping to reduce incidence of chilling injury (Xi
660 et al., 2012). Follow-up studies should therefore focus on these aspects important conditions.

661 The CMTC depicted in Figure 13a shows the potential rate of moisture transport between the
662 board and air regions as determined by the flow properties near the board surface. It should be
663 noted, however, the mass transfer Biot number was about 100, indicating a low dependence on
664 convective transport. The average CMTC was 5.1×10^{-3} m s^{-1} for the carton surfaces in contact
665 with the pallet base (bottom surface), where flow was highest and 3.8×10^{-3} m s^{-1} at the inner
666 carton surfaces, which had comparatively lower flow rates. The CMTC was relatively evenly
667 distributed along the carton surfaces (Figure 13a), except near the vent holes, where CMTC
668 values were considerably larger (2.5×10^{-2} m s^{-1} to 6.3×10^{-2} m s^{-1}).

669 An important consideration is that there are three moisture related factors influencing carton
670 strength. First, the high board moisture concentration, which weaken the board by breaking
671 hydrogen bonds in the cellulose. Second, the heterogeneous moisture content gradients
672 throughout the cartons at any moment, resulting in inhomogeneous hygro-expansion
673 throughout the stack. Third, the transient changes in moisture content over time in combination
674 with the large compression forces result in a process of mechano-sorptive creep. The study
675 showed that the relatively large heat capacity of fruit packed inside cartons can buffer sudden
676 board temperature changes, which if not present may have influenced a_w (EMC). Similarly,
677 compared to the air, the board itself has a large moisture capacity, which also buffers changes
678 to the airs RH. Consequently, board that is at EMC with respect to the shipping conditions, can
679 provide moisture under drying conditions and adsorb moisture as the air humidity increases.

680 ## 4. Future research

681 Many important moisture processes within corrugated packaging during optimal shipping
682 conditions were investigated and these provide useful base-line information for future
683 investigations. Future work should thus aim to investigate the moisture spatio-temporal
684 changes within cartons during non-optimal shipping conditions, which are needed for the
685 development of improved packaging designs. For instance, the effect of cold chain breaks is
686 expected to decrease carton strength as a result creep processes in the board. Cold chain breaks
687 could consequently lead to large temperature gradients across the RFC, as well as increased
688 fruit respiration and transpiration rates. Additionally, the potentially impact on moisture loss

when loading RFCs with dry cartons is another import subject, and has not been considered in prior studies. Specifically, dry cartons would initially adsorb much of the available moisture inside a container, resulting in larger fruit moisture loss rates than normal.

Future follow-up research could also improve on the proposed model. For example, the incorporation of condensation physics into the model may be necessary under cold chain breaks. Additionally, more detailed simulations may require more comprehensive validation experiments. To this end, a promising technology to measure moisture processes in detail is neutron radiography, which provides a very high dynamic range (Defraeye et al., 2016). This is due to the neutron beams, which are attenuated strongly by hydrogen and thus sensitive to water molecules. However, application of neutron radiography requires extensive use of specialised equipment, such as nuclear reactors, which will need to be used over extended time periods to observe the relatively slow moisture transport processes.

Finally, the respective model could also be further developed to predict the effect of spatio-temporal changes in moisture content on mechano-sorptive creep. Possible approaches include linking the respective CFD model's outputs to a mechanical-finite element model (FEM). Alternatively, the physics of this respective model could be incorporated into a multi-physic FEM model. Currently, approaches to model the mechano-sorptive creep process have been limited and most efforts have been focused on experimental research at small (e.g. individual fibres) scales (Huč et al., 2018; Olsson et al., 2007; Olsson and Salmén, 2014).

5. Conclusions

Stacked corrugated fibreboard cartons are transported in refrigerated freight containers (RFC) at low temperatures and high humidity conditions. The resulting presence of high moisture contents and moisture gradients in the corrugated fibreboard cartons can have a substantial effect on carton mechanical strength. This study has characterised moisture properties in stacked cartons under standard shipping conditions. To achieve this, a CFD model was developed to predict moisture transport through stacked cartons under convective airflow conditions. The CFD model was validated using two experimental approaches which compared well with model predictions. The study incorporated the presence of respiration, transpiration, defrost cycles, initial RFC activation and temperature changes over the typical voyage for exporting fresh fruit from South Africa to United Kingdom.

Results revealed relatively small spatio-temporal changes in moisture content under standard shipping conditions, with the board moisture content decreasing by 0.4 g/100$g_{dry\ fibre}$ over the simulation period (7-days). Little effect from the daily defrost cycles was observed on board moisture content. The initial RFC activation (refrigeration is powered on), whereby the warm air around the container walls was forced up into the pallet stack, caused a rapid change in RH and therefore accelerated the development of a heterogeneous moisture content distribution. The temperature gradient caused by heat conduction from outside through the container wall was the most significant factor affecting spatio-temporal changes in moisture content. By day 7, a moisture content gradient of 0.6 g/100$g_{dry\ fibre}$ was observed across the domain (3 cartons). Although relatively small, these gradients are expected to have some contribution to the creep process and would be considerably more prevalent during cold chain breaks. The effect of these moisture content gradients should thus be quantified with respect to mechanical strength in future studies. The model can therefore provide valuable insight into the mechano-sportive creep process and potentially guide the development of future testing approaches and package designs.

Acknowledgments

This work was based upon research supported by the South African Research Chairs Initiative of the Department of Science and Technology and National Research Foundation. The Postharvest Innovation Programme (PHI) and Hortgro Science partially supported the development of this project. Corrugated fibreboard samples were attained from A P L Cartons, Worcester, South Africa and the authors thank the staff for their invaluable support and assistance. Computations were performed using the University of Stellenbosch's Rhasatsha HPC: http://www.sun.ac.za/hpc. We also acknowledge the support of the Swiss National Science Foundation SNSF (project 200021_169372). The authors would like to thank the Coop Research Program of the ETH Zurich World Food System Center and the ETH Foundation.

References

Alfthan, J., 2004. The effect of humidity cycle amplitude on accelerated tensile creep of paper. Mech. Time-Dependent Mater. 8, 289–302.

Alfthan, J., 2003. A simplified network model for mechano-sorptive creep in paper. J. Pulp Pap.

749 Sci. 29, 228–234.

750 Alfthan, J., Gudmundson, P., Östlund, S., 2002. A micro-mechanical model for mechano-
751 sorptive creep in paper. J. Pulp Pap. Sci. 28, 98–104.

752 Allaoui, S., Aboura, Z., Benzeggagh, M.L., 2009. Phenomena governing uni-axial tensile
753 behaviour of paperboard and corrugated cardboard. Compos. Struct. 87, 80–92.
754 https://doi.org/10.1016/j.compstruct.2008.01.001

755 Ambaw, A., Delele, M.A., Defraeye, T., Ho, Q.T., Opara, U.L., Nicolaï, B.M., Verboven, P.,
756 2013a. The use of CFD to characterize and design post-harvest storage facilities: Past,
757 present and future. Comput. Electron. Agric. 93, 184–194.
758 https://doi.org/10.1016/j.compag.2012.05.009

759 Ambaw, A., Mukama, M., Opara, U.L., 2017. Analysis of the effects of package design on the
760 rate and uniformity of cooling of stacked pomegranates: Numerical and experimental
761 studies. Comput. Electron. Agric. 136, 13–24.
762 https://doi.org/10.1016/j.compag.2017.02.015

763 Ambaw, A., Verboven, P., Defraeye, T., Tijskens, E., Schenk, A., Opara, U.L., Nicolaï, B.M.,
764 2013b. Porous medium modeling and parameter sensitivity analysis of 1-MCP distribution
765 in boxes with apple fruit. J. Food Eng. 119, 13–21.
766 https://doi.org/10.1016/j.jfoodeng.2013.05.007

767 Ambaw, A., Verboven, P., Defraeye, T., Tijskens, E., Schenk, A., Opara, U.L., Nicolaï, B.M.,
768 2013c. Effect of box materials on the distribution of 1-MCP gas during cold storage: A
769 CFD study. J. Food Eng. 119, 150–158. https://doi.org/10.1016/j.jfoodeng.2013.05.019

770 Ambaw, A., Verboven, P., Delele, M.A., Defraeye, T., Tijskens, E., Schenk, A., Verlinden, B.E.,
771 Opara, U.L., Nicolaï, B.M., 2014. CFD-based analysis of 1-MCP distribution in
772 commercial cool store rooms: Porous medium model application. Food Bioprocess
773 Technol. 7, 1903–1916. https://doi.org/10.1007/s11947-013-1190-9

774 Armstrong, L.D., Christensen, G.N., 1961. Influence of moisture changes on deformation of
775 wood under stress. Nature 191, 869–870.

776 Armstrong, L.D., Kingston, R.S.T., 1960. Effect of moisture changes on creep in wood. Nature
777 185, 862–863.

778 ASHRAE, 2009. ASHRAE Handbook - Fundamentals (SI edition). American Society of
779 Heating, Refrigerating and Air Conditioning Engineers, Inc, Atlanta, GA, USA.

780 ASHRAE, 2006. Refrigeration Load, in: ASHRAE Handbook Refrigeration (SI). American
781 Society of Heating, Refrigerating and Air Conditioning Engineers, Inc, Atlanta, GA, USA,
782 p. 13.1-13.8.

783 ASHRAE, 2000. ASHRAE Handbook - HVAC systems and Equipment (SI edition). American
784 Society of Heating, Refrigerating and Air Conditioning Engineers, Inc, Atlanta, GA, USA.

785 Bandyopadhyay, A., Radhakrishnan, H., Ramarao, B. V, Chatterjee, S.G., 2000. Moisture
786 sorption response of paper subjected to ramp humidity changes: Modeling and
787 experiments. Ind. Eng. Chem. Res. 39, 219–226. https://doi.org/10.1021/ie990279w

788 Bandyopadhyay, A., Ramarao, B. V, Ramaswamy, H.S., 2002. Transient moisture diffusion
789 through paperboard materials. Colloids Surfaces A Physicochem. Eng. Asp. 206, 455–
790 467. https://doi.org/10.1016/S0927-7757(02)00067-5

Basu, S., Shivhare, U.S., Mujumdar, A.S., 2006. Models for Sorption Isotherms for Foods: A Review. Dry. Technol. 24, 917–930. https://doi.org/10.1080/07373930600775979

Becker, B.R., Misra, A., Fricke, B.A., 1996. Bulk refrigeration of fuits and vegatables part I : Theoretical consideration of heat. HVAC&R Res. 2, 122–134.

Berry, T.M., Delele, M.A., Griessel, H., Opara, U.L., 2015. Geometric design characterisation of ventilated multi-scale packaging used in the South African pome fruit industry. Agric. Mech. Asia, Africa, Lat. Am. 46, 1–19.

Berry, T.M., Fadiji, T.S., Defraeye, T., Opara, U.L., 2017. The role of horticultural carton vent hole design on cooling efficiency and compression strength: A multi-parameter approach. Postharvest Biol. Technol. 124, 62–74. https://doi.org/10.1016/j.postharvbio.2016.10.005

Bronlund, J.E., Redding, G.P., Robertson, T.R., 2014. Modelling steady-state moisture transport through corrugated fibreboard packaging. Packag. Technol. Sci. 27, 193–201. https://doi.org/10.1002/pts.2025

Brosnan, T., Sun, D.-W., 2001. Precooling techniques and applications for horticultural products—a review. Int. J. Refrig. 24, 154–170.

Byrd, V.L., 1972a. Effect of relative humidity changes on compressive creep response of paper. Tappi 55, 1612–1613.

Byrd, V.L., 1972b. Effect of relative humidity changes during creep on handsheet paper properties. Tappi 55, 247–252.

Celik, I.B., Ghia, U., Roache, P.J., Freitas, C.F., Coleman, H., Raad, P.E., 2008. Procedure for estimation and reporting of uncertainty due to discretization in CFD applications. J. Fluids Eng. 130, 1–4. https://doi.org/10.1115/1.2960953

Chatterjee, S.G., 2001. Comparison of domain and similarity models for characterizing moisture sorption equilibria of paper. Ind. Eng. Chem. Res. 40, 188–194. https://doi.org/10.1021/ie000437f

Chatterjee, S.G., Ramarao, B. V, Tien, C., 1997. Water-vapour sorption equilibria of a bleached-kraft paperboard - A study of the hysteresis region. J. Pulp Pap. Sci. 23, J366–J373.

Chau, K. V, Romero, R.A., Baird, C.D., Gaffney, J.J., 1987. Transpiration Coefficients of Fruits and Vegetables in Refrigerated Storage. ASHRAE Reports 370–380.

Chourasia, M.K., Goswami, T.K., 2007. Three dimensional modeling on airflow, heat and mass transfer in partially impermeable enclosure containing agricultural produce during natural convective cooling. Energy Convers. Manag. 48, 2136–2149. https://doi.org/10.1016/j.enconman.2006.12.018

Cleland, D.J., Tanner, D.J., Bronlund, J.E., Merts, I., 2008. Rates of moisture sorption from food packaging materials. ASHRAE Trans. 114, 252(12).

Darling, R.C., Belding, H., 1946. Moisture adsorption of textile yarns at low temperatures. J. Textle Inst. 38, 524–529. https://doi.org/10.1021/ie50437a023

Defraeye, T., Cronjé, P., Verboven, P., Opara, U.L., Nicolaï, B.M., 2015. Exploring ambient loading of citrus fruit into reefer containers for cooling during marine transport using computational fluid dynamics. Postharvest Biol. Technol. 108, 91–101. https://doi.org/10.1016/j.postharvbio.2015.06.004

832 Defraeye, T., Nicolaï, B.M., Mannes, D., Aregawi, W.A., Verboven, P., Derome, D., 2016.
833 Probing inside fruit slices during convective drying by quantitative neutron imaging. J.
834 Food Eng. 178, 198–202. https://doi.org/10.1016/j.jfoodeng.2016.01.023

835 Delele, M.A., Ngcobo, M.E.K., Opara, U.L., Meyer, C.J., 2012. Investigating the effects of
836 table grape package components and stacking on airflow, heat and mass transfer using 3-
837 D CFD modelling. Food Bioprocess Technol. 6, 2571–2585.
838 https://doi.org/10.1007/s11947-012-0895-5

839 Delele, M.A., Schenk, A., Tijskens, E., Ramon, H., Nicolaï, B.M., Verboven, P., 2009.
840 Optimization of the humidification of cold stores by pressurized water atomizers based on
841 a multiscale CFD model. J. Food Eng. 91, 228–239.
842 https://doi.org/10.1016/j.jfoodeng.2008.08.027

843 Delele, M.A., Verboven, P., Ho, Q.T., Nicolaï, B.M., 2010. Advances in mathematical
844 modelling of postharvest refrigeration processes. Stewart Postharvest Rev. 6, 1–8.
845 https://doi.org/10.2212/spr.2010.2.1

846 Fadiji, T., Coetzee, C., Opara, U.L. 2016. Compression strength of ventilated corrugated
847 paperboard packages: Numerical modelling, experimental validation and effects of vent
848 geometric design. Biosystems Engineering, 151:231-247.
849 http://dx.doi.org/10.1016/j.biosystemseng.2016.09.010

850 Fadiji, T., Berry, T.M., Coetzee, C., Opara, U.L. 2018. Mechanical design and performance
851 testing of corrugated paperboard packaging for the postharvest handling of horticultural
852 produce. Biosystems Engineering, 171:220-244.
853 https://doi.org/10.1016/j.biosystemseng.2018.05.004

854 FEFCO, ESBO, 2007. International fibreboard case code. FEFCO, Belgium.

855 Geankoplis, C.J., 1978. Transport Processes and Unit Operations. Allyn and Bacon, Boston.

856 Gibson, E.J., 1965. Role of water and effect of a changing moisture content. Nature 206, 213–
857 215.

858 Greenspan, L., 1977. Humidity fixed points of binary saturated aqueous solutions. J. Res. Natl.
859 Bur. Stand. (1934). 81A, 89–96. https://doi.org/10.6028/jres.081A.011

860 Habeger, C.C., Coffin, D.W., 2000. The role of stress concentrations in accelerated creep and
861 sorption induced physical aging. J. Pulp Pap. Sci. 26, 145–157.

862 Haslach, H.W., 2000. The moisture and rate-dependent mechanical properties of paper : A
863 review. Mech. Time-Dependant Mater. 4, 169–210.
864 https://doi.org/10.1023/A:1009833415827

865 Haslach, H.W., 1994. The mechanics of moisture accelerated tensile creep in paper. TAPPI J.
866 70, 179–186.

867 Hassanizadeh, M., Gray, W.G., 1979. General conservation equations for multi-phase systems:
868 1. Averaging procedure. Adv. Water Resour. 2, 131–144. https://doi.org/10.1016/0309-
869 1708(79)90025-3

870 Hoang, H.-M., Duret, S., Flick, D., Laguerre, O., 2015. Preliminary study of airflow and heat
871 transfer in a cold room filled with apple pallets: Comparison between two modelling
872 approaches and experimental results. Appl. Therm. Eng. 76, 367–381.
873 https://doi.org/10.1016/j.applthermaleng.2014.11.012

874 Huč, S., Svensson, S., Hozjan, T., 2018. Numerical Modeling of Timber Structures under
875 Varying Humidity Conditions. Int. J. Civ. Environ. Eng. 5. https://doi.org/10.1999/1307-
876 6892/81491

877 Kessler, H., Stoll, K., 1953. Versuchsergebnisse bei der kaltlagerung von apfelsorten. Landw.
878 Jb. Schweiz 1157–1184.

879 Labuza, T.P., Altunakar, B., 2007. Water Activity Predictions and Moisture Sorption Isotherms,
880 in: Barbosa-Canovas, G. V, Fontana, A.J., Schmidt, S.J., Labuza, T.P. (Eds.), Water
881 Activity in Foods. Blackwell Publishing, Carlton, Australia.

882 Marcondes, J., 1996. Corrugated fibreboard in modified atmospheres : Moisture
883 sorption/desorption and shock cushioning. Packag. Technol. Sci. 9, 87–98.

884 Menter, F.R., 1994. Two-equation eddy-viscosity turbulence models for engineering
885 applications. AIAA J. 32, 1598–1605. https://doi.org/10.2514/3.12149

886 Mualem, Y., 1973. Modified approach to capillary hysteresis based on a similarity hypothesis.
887 Water Resour. Res. 9, 1324–1331. https://doi.org/10.1029/WR009i005p01324

888 Ngcobo, M.E.K., Delele, M.A., Opara, U.L., Zietsman, C.J., Meyer, C.J., 2012. Resistance to
889 airflow and cooling patterns through multi-scale packaging of table grapes. Int. J. Refrig.
890 35, 445–452. https://doi.org/10.1016/j.ijrefrig.2011.11.008

891 Norton, T., Sun, D.-W., Grant, J., Fallon, R., Dodd, V., 2007. Applications of computational
892 fluid dynamics (CFD) in the modelling and design of ventilation systems in the
893 agricultural industry: A review. Bioresour. Technol. 98, 2386–2414.
894 https://doi.org/http://dx.doi.org/10.1016/j.biortech.2006.11.025

895 Olsson, A.-M., Salmén, L., 2014. Mechano-sorptive creep in pulp fibres and paper. Wood Sci.
896 Technol. 48, 569–580. https://doi.org/10.1007/s00226-014-0624-5

897 Olsson, A.-M., Salmén, L., Eder, M., Burgert, I., 2007. Mechano-sorptive creep in wood fibres.
898 Wood Sci. Technol. 41, 59–67. https://doi.org/10.1007/s00226-006-0086-5

899 Parker, M.E., Bronlund, J.E., Mawson, A.J., 2006. Moisture sorption isotherms for paper and
900 paperboard in food chain conditions. Packag. Technol. Sci. 193–209.
901 https://doi.org/10.1002/pts

902 Pathare, P.B., Opara, U.L., Vigneault C, Delele M, Al-Said F A 2012. Design of packaging vents
903 for cooling fresh horticultural produce. Food and Bioprocess Technology, 5(6): 2031-
904 2045. Doi: 10.1007/s11947-012-0883-9

905 Pathare, P.B., Opara U.L. 2014. Structural design of corrugated boxes for horticultural
906 produce: A review. Biosystems Engineering 125; 128-140.
907 http://dx.doi.org/10.1016/j.biosystemseng.2014.06.021

908 Pathare, P.B., Berry, T.M., Opara, U.L., 2016. Changes in moisture content and compression
909 strength during storage of ventilated corrugated packaging used for handling apples.
910 Packag. Res. 1, 1–6. https://doi.org/10.1515/pacres-2016-0001

911 Peleg, M., 1993. Assessment of a semi-empirical four parameter general model for sigmid
912 moisture sorption isotherms. J. Food Eng. 16, 21–37.

913 Peralta, P.N., Bangi, A.P., 1998. Modeling wood moisture sorption hysteresis based on
914 similarity hypothesis. Part 2. Capillary_Radii approach. Wood Fiber Sci. 30, 148–154.

915 Radhakrishnan, H., Chatterjee, S.G., Ramarao, B. V, 2000. Steady-state moisture transport in
916 a bleached kraft paperboard stack. J. pulp Pap. Sci. 26, 140–144.

917 Rahman, A.A., Urbanik, T.J., Mahamid, M., 2006. FE analysis of creep and hygroexpansion
918 response of a corrugated fiberboarad to a moisture flow: A transient nonlinear analysis.
919 Wood Fiber Sci. 38, 268–277.

920 Ramaswamy, H.S., Tung, M.A., 1981. Thermophysical properties of apples in relation to
921 freezing. J. Food Sci. 46, 724–728. https://doi.org/10.1111/j.1365-2621.1981.tb15335.x

922 Roache, P.J., 1994. Perspective: a method for uniform reporting of grid refinement studies. J.
923 Fluids Eng. 116, 405–413.

924 Robertson, G.L., 2013. Food Packaging: Principles and Practice, 2nd ed. CRC Press: Boca
925 Raton, Boca-Raton.

926 Skogman, R.E.T., Scheie, C.E., 1969. The effect of temperature on the moisture adsorption of
927 kraft paper. Tappi J. 52, 489–490.

928 Smale, N.J., Moureh, J., Cortella, G., 2006. A review of numerical models of airflow in
929 refrigerated food applications. Int. J. Refrig. 29, 911–930.

930 Söremark, C., Fellers, C., 1993. Mechano-sorptive creep and hygroexpansion of corrugated
931 board in bending. J. Pulp Pap. Sci. 19, J19–J26.

932 Sørensen, G., Hoffmann, J., 2003. Moisture sorption in moulded fibre trays and effect on static
933 compression strength. Packag. Technol. Sci. 16, 159–169. https://doi.org/10.1002/pts.622

934 TAPPI, 2012. T804: Compression test of fiberboard shipping containers., Resource book.
935 International Safe Transit Association.

936 Thompson, J.F., Mitchell, F.G., Rumsey, T.R., Kasmire, R.F., Crisosto, C.H., 2008.
937 Commercial Cooling of Fruits, Vegetables, and Flowers, Revised. ed. University of
938 California Department of Agriculture and Natural Resources, Oakland, California.

939 USDA, 1986. Commercial storage of fruits vegetables and florist and nursery stocks, in:
940 Agricultural Handbook Number 66. United States Department of Agriculture.

941 van der Sman, R.G.M., 2003. Simple model for estimating heat and mass transfer in regular-
942 shaped foods. J. Food Eng. 60, 383–390. https://doi.org/10.1016/S0260-8774(03)00061-
943 X

944 Wahba, M., Nashed, S., 1957. Moisture relations of cellulose. J. Textle Inst. 48, T1–T20.

945 Xi, W., Zhang, B., Shen, J., Sun, C., Xu, C., Chen, K., 2012. Intermittent warming alleviated
946 the loss of peach fruit aroma-related esters by regulation of AAT during cold storage.
947 Postharvest Biol. Technol. 74, 42–48. https://doi.org/10.1016/j.postharvbio.2012.07.003

948 Zhao, C.-J., Han, J.-W., Yang, X.-T., Qian, J.-P., Fan, B.L., 2016. A review of computational
949 fluid dynamics for forced-air cooling process. Appl. Energy 168, 314–331.
950 https://doi.org/10.1016/j.apenergy.2016.01.101

951

952

Tables

Table 1: Overview of the four different apparatus/devices used in this study and how they were applied in experiments and CFD models.

	Measurement experiments	Validation experiments	CFD models
Diffusion cup	Determine corrugated fibreboard moisture diffusion properties.		
Glass-chamber	Determine equilibrium moisture content (EMC) curves at various conditions.	Evaluation of board moisture content under varying relative humidity under diffusion only conditions.	Comparative numerical evaluation of board moisture content under varying relative humidity under diffusion only conditions.
CATTS-chamber		Evaluation of board moisture content under varying relative humidities and temperatures under convection-diffusion conditions.	Comparative numerical evaluation of board moisture content under varying relative humidities and temperatures under convection-diffusion conditions.
Refrigerated freight container	Determine conditions inside a fully loaded RFC during shipment (for CFD model setup).		Investigation of carton spatio-temporal moisture contents inside a refrigerated freight container during shipping.

Table 2: Average temperature and relative humidity conditions (SD < 5%) in the CATTS-chamber at the moments when conditions were cycled and samples were extracted for measurement.

Hours into experiment	Temperature	Relative humidity
0	25 °C	59 %
7.9	33 °C	94 %
12.3	25 °C	47 %
17.3	32 °C	95 %
21.4	25 °C	32 %

Table 3: Physical and diffusivity parameters of the C-flute corrugated board.

Parameter	20 °C	1 °C
Liner fibreboard (outer side) thickness	407 µm	407 µm
Liner fibreboard (inner inner) thickness	357 µm	357 µm
Fluting fibreboard thickness	317 µm	317 µm
Effective thickness of air component in CF	3 023 µm	3 023 µm
Corrugated fibreboard (CF) thickness	4 244 µm	4 244 µm
CF take up factor[a]	1.44	1.44
Diffusivity of air (D_a) [b]	2.50×10^{-5} m^2 s^{-1}	2.19×10^{-5} m^2 s^{-1}

Inter-fibre diffusivity (pore regions; D_p)[c]	5.07×10^{-7} m^2 s^{-1}	5.07×10^{-7} m^2 s^{-1}
Total effective diffusivity across CF (D_{eff}) [d]	2.62×10^{-6} m^2 s^{-1}	3.43×10^{-6} m^2 s^{-1}
Effective diffusivity across CF inter-fibre regions and air gaps ($D_{eff,p}$)	1.68×10^{-6} m^2 s^{-1}	1.67×10^{-6} m^2 s^{-1}
Effective diffusivity across CF fibre regions ($D_{eff,q}$)	9.44×10^{-7} m^2 s^{-1}	1.76×10^{-6} m^2 s^{-1}

962 [a] Ratio between the fluting and liner fibreboard surface areas;
963 [b] As taken from ASHRAE (2009);
964 [c] As taken from Bandyopadhyay et al. (2002);
965 [d] Experimentally determined, SD = 4% (relative standard deviation).
966

Figures

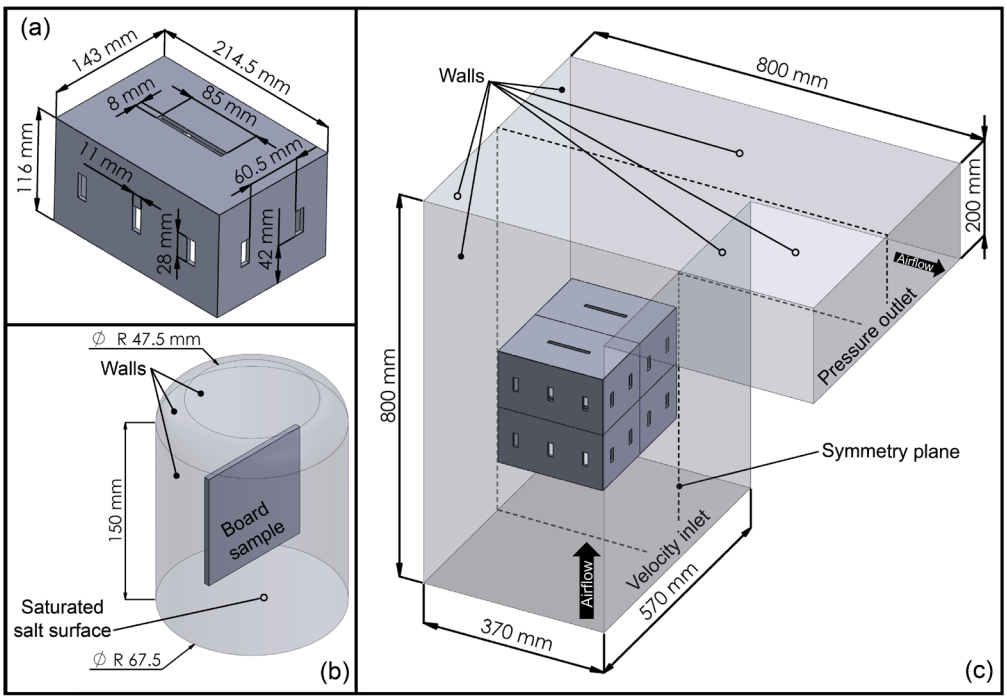

Figure 1: Schematic diagram showing geometry and boundary conditions of the (a) small scale carton, (b) glass-chamber and (c) CATTS-chamber, dashed line indicates symmetry plane.

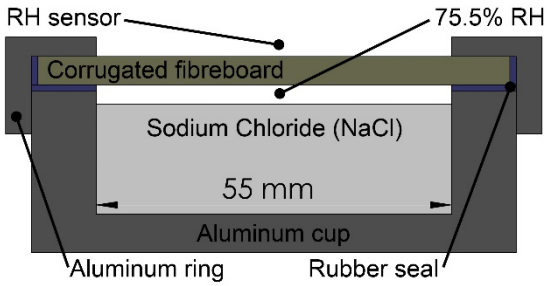

Figure 2: Cross section diagram of the diffusion cup setup. An average relative humidity (RH) of 84.4% was maintained just above the board sample, by holding the diffusion cup in a sealed glass-chamber containing a solution saturated with Potassium nitrate (KNO_3; 94.6% RH).

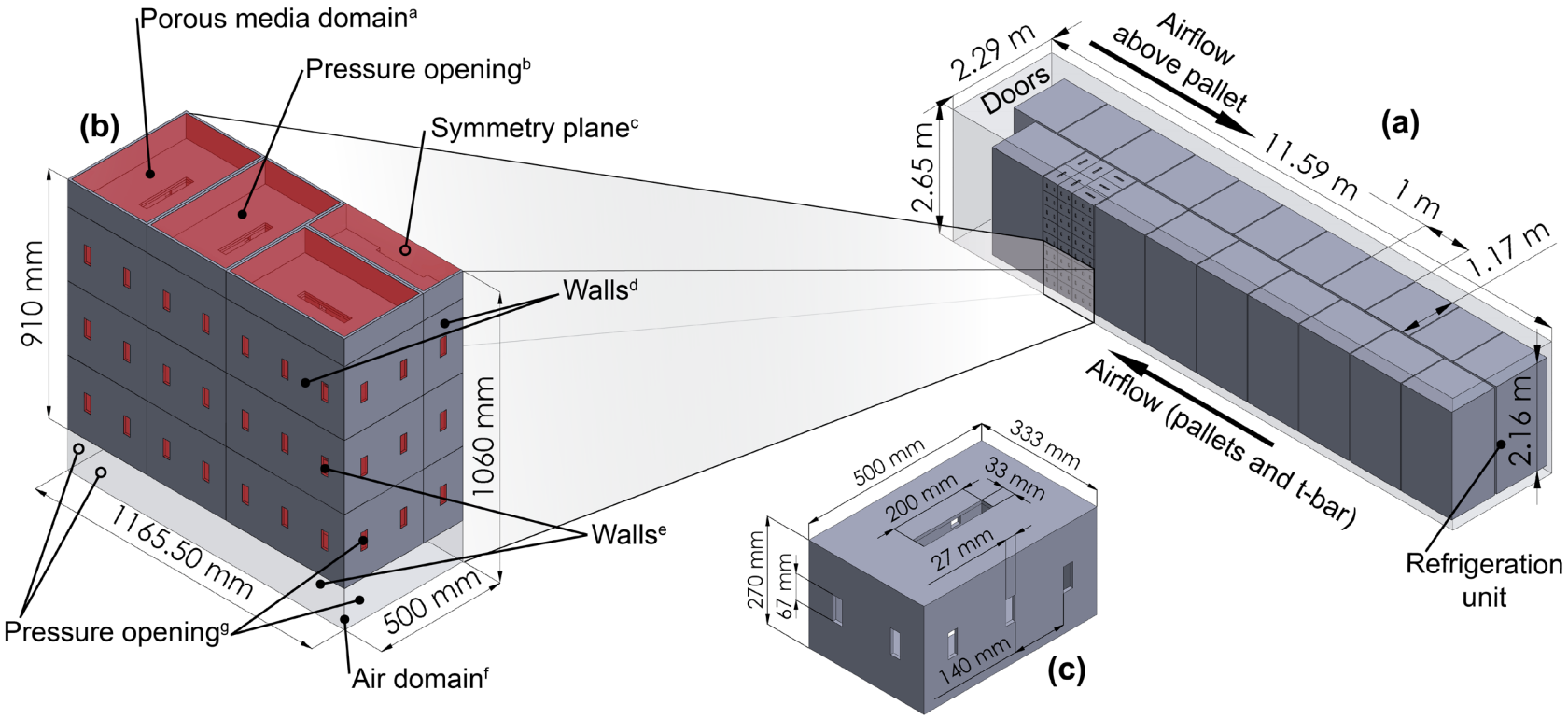

Figure 3: Schematic diagram of the (a) refrigerated shipping container, which depicts the (b) simulation domain used in this study. Superscript letters indicate: [a] air and fruit filled volume (red region); [b] top boundaries along the porous media domain; [c] vertical boundaries (carton and porous media) through the pallet; [d] all outer carton surfaces; [e] vertical boundaries along the reefer container wall at vent holes and air domain; [f] air volume (under cartons) representing pallet; [g] front, back and bottom boundaries along the air domain. Diagram (c) shows geometric specification of the ventilated carton used in the pallet stack.

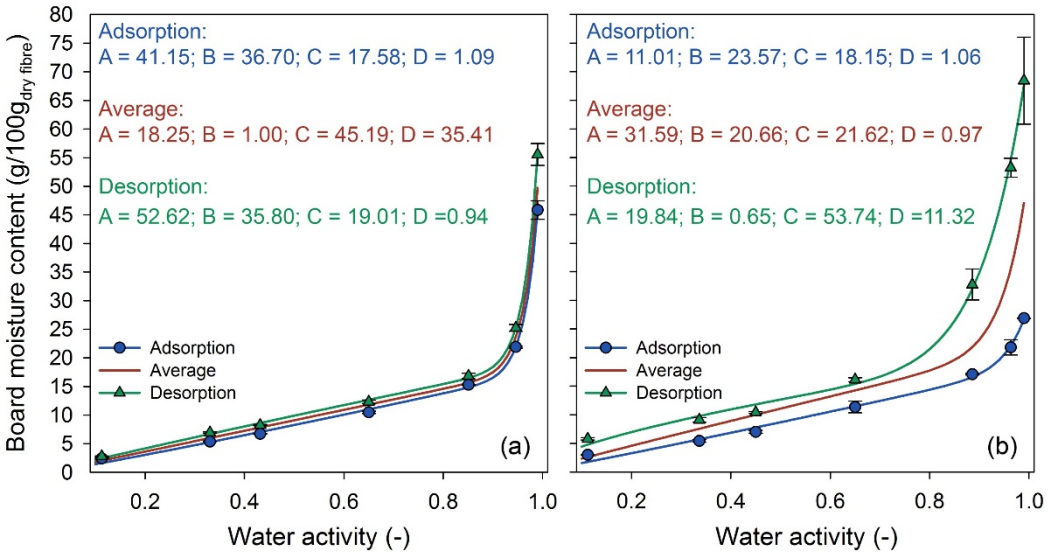

Figure 4: Equilibrium moisture content for the corrugated fibreboard used in this study, with respect to the water activity for the adsorption, desorption and average (of the two) curves at (a) 20 ºC and (b) 1 ºC. The A-D values represent the corresponding coefficients for the Peleg equation (Eq. (14)).

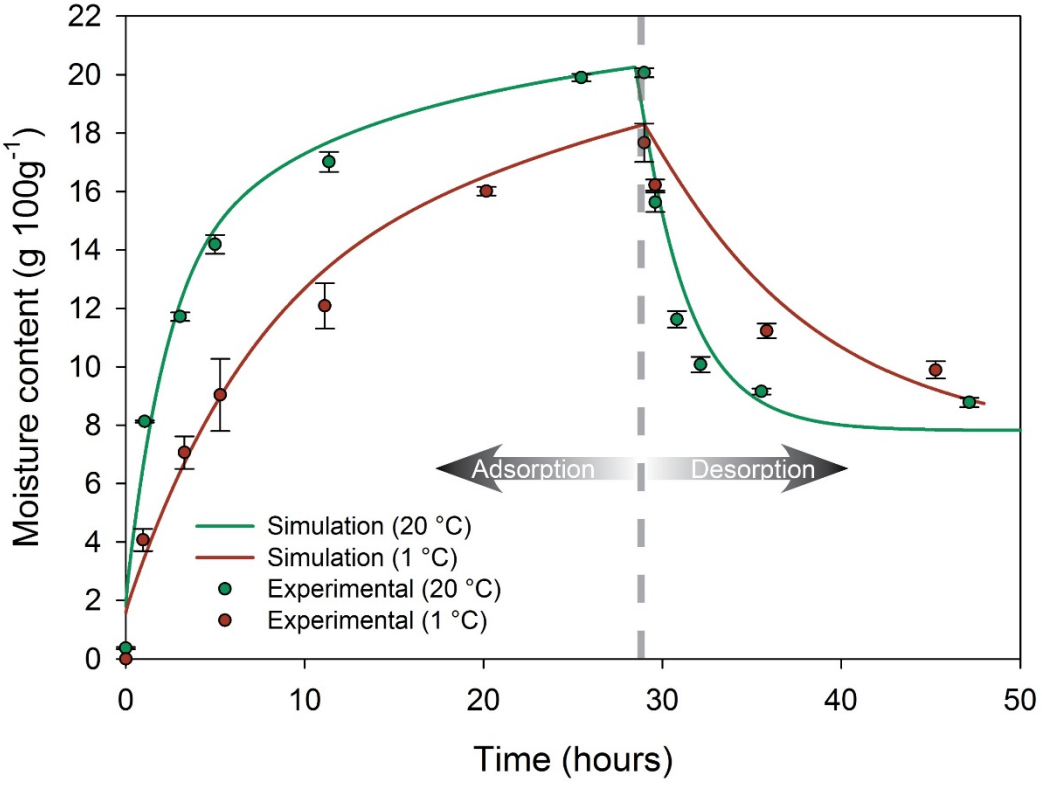

Figure 5: Comparison between experimental and numerical moisture content values of a corrugated fibreboard sample stored in the glass-chamber over time. All error bars indicate standard deviation of the mean.

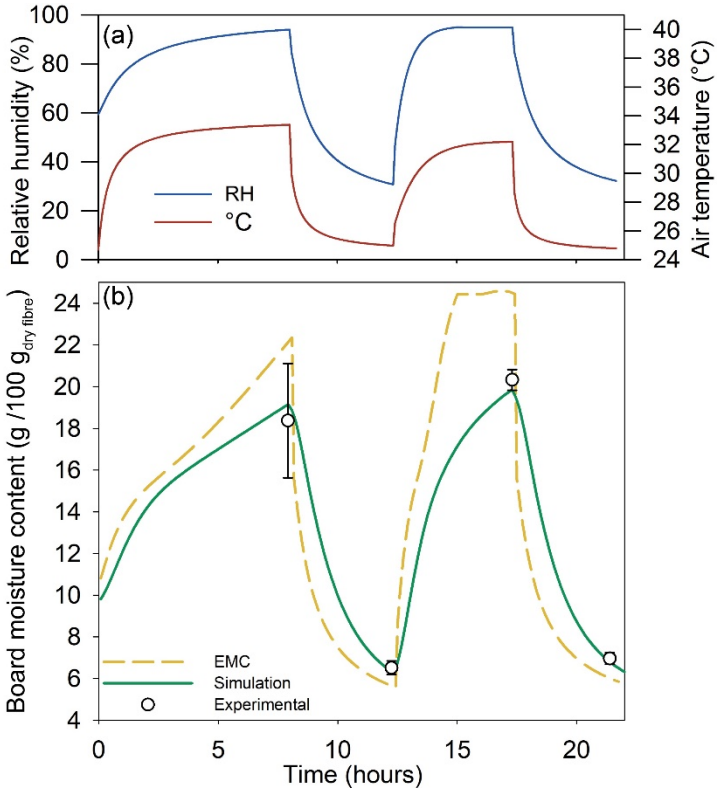

Figure 6: (a) Applied temperature and relative humidity conditions and (b) comparisons between experimental and simulation results for the CATTS validation experiment. The yellow (dashed) line indicates the equilibrium moisture content (EMC) of the cartons, based on the average PELEG model and the RH at the inlet. Error bars indicate standard error of the mean.

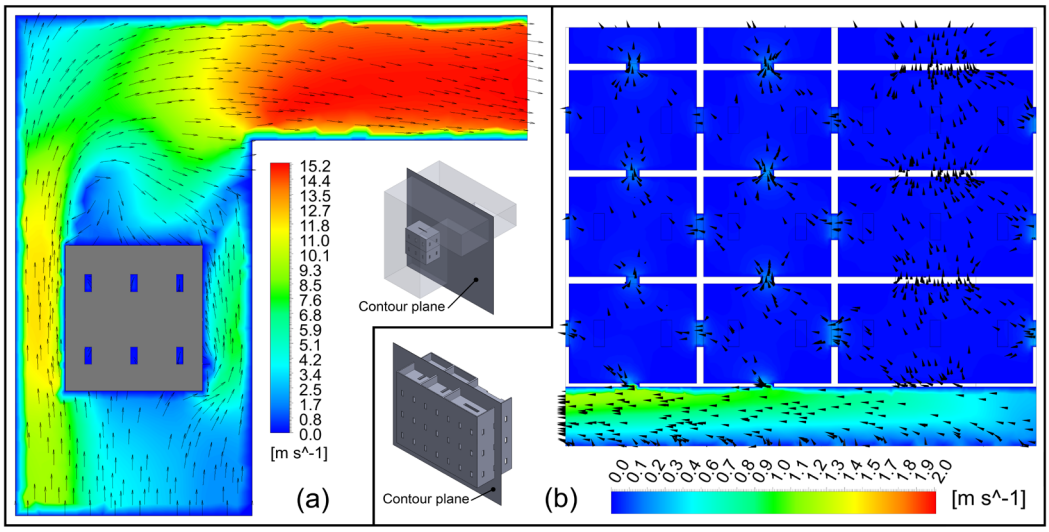

Figure 7: Simulated contours of velocity profile along the (a) symmetry plane of the CATTS-chamber and (b) through the centre plane of the pallet domain.

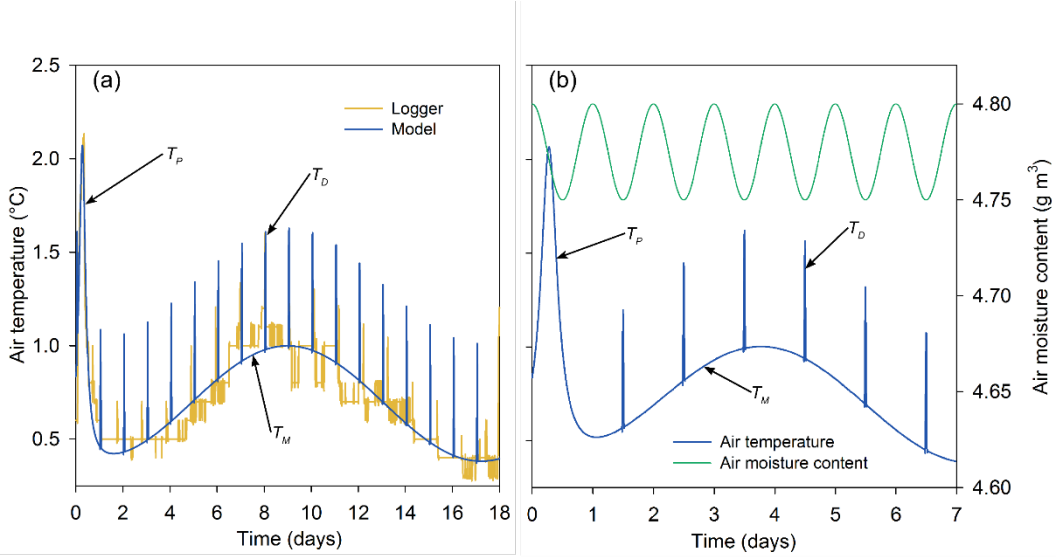

Figure 8: (a) Average logger and model air temperature inside a pallet shipped from South Africa to the United Kingdom over 18-days. (b) Shows the seven day simplification of the full (18-day) shipping duration and indicates the temperature and moisture values used at the pressure openings of the pallet stack over the RFC simulation period.

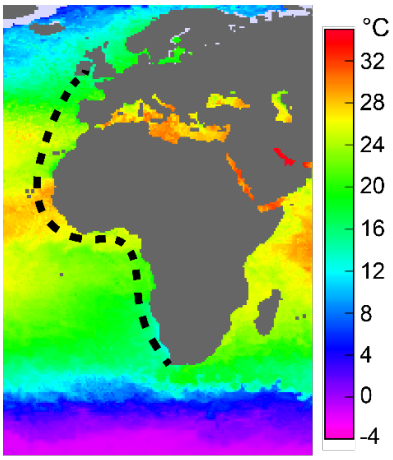

Figure 9: Sea Surface Temperature (SST) data produced for the 24th of August 2015. Dashed line indicates the shipping journey between South Africa and UK, each dash represents one of the 18 travel days. Data acquired from the NASA Jet propulsion laboratory ROMS (Regional Ocean Modelling System) group (http://ourocean.jpl.nasa.gov/SST).

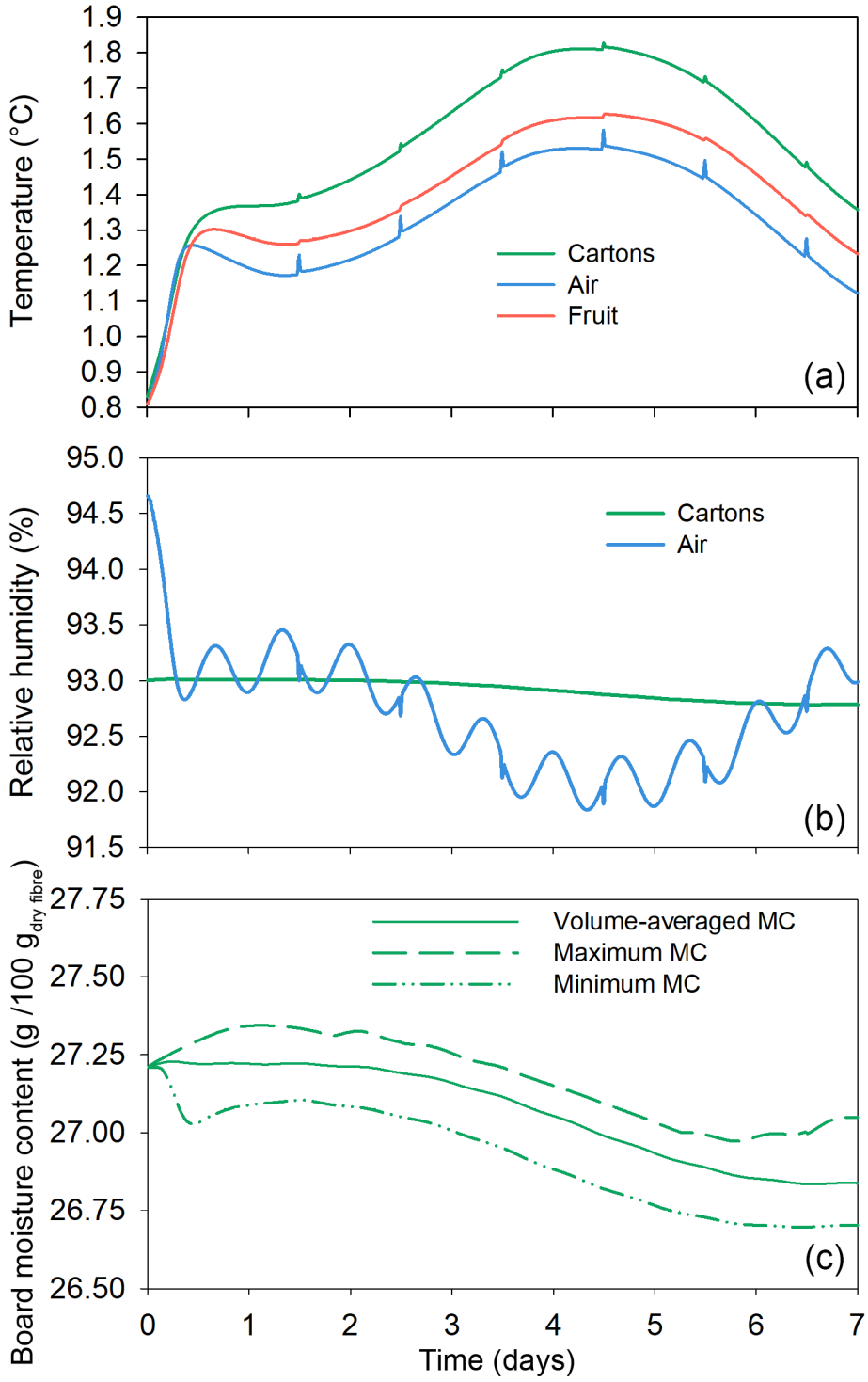

Figure 10: (a) Average temperature, (b) relative humidity and (c) moisture content (MC) in cartons and porous regions over the 7-day shipping period.

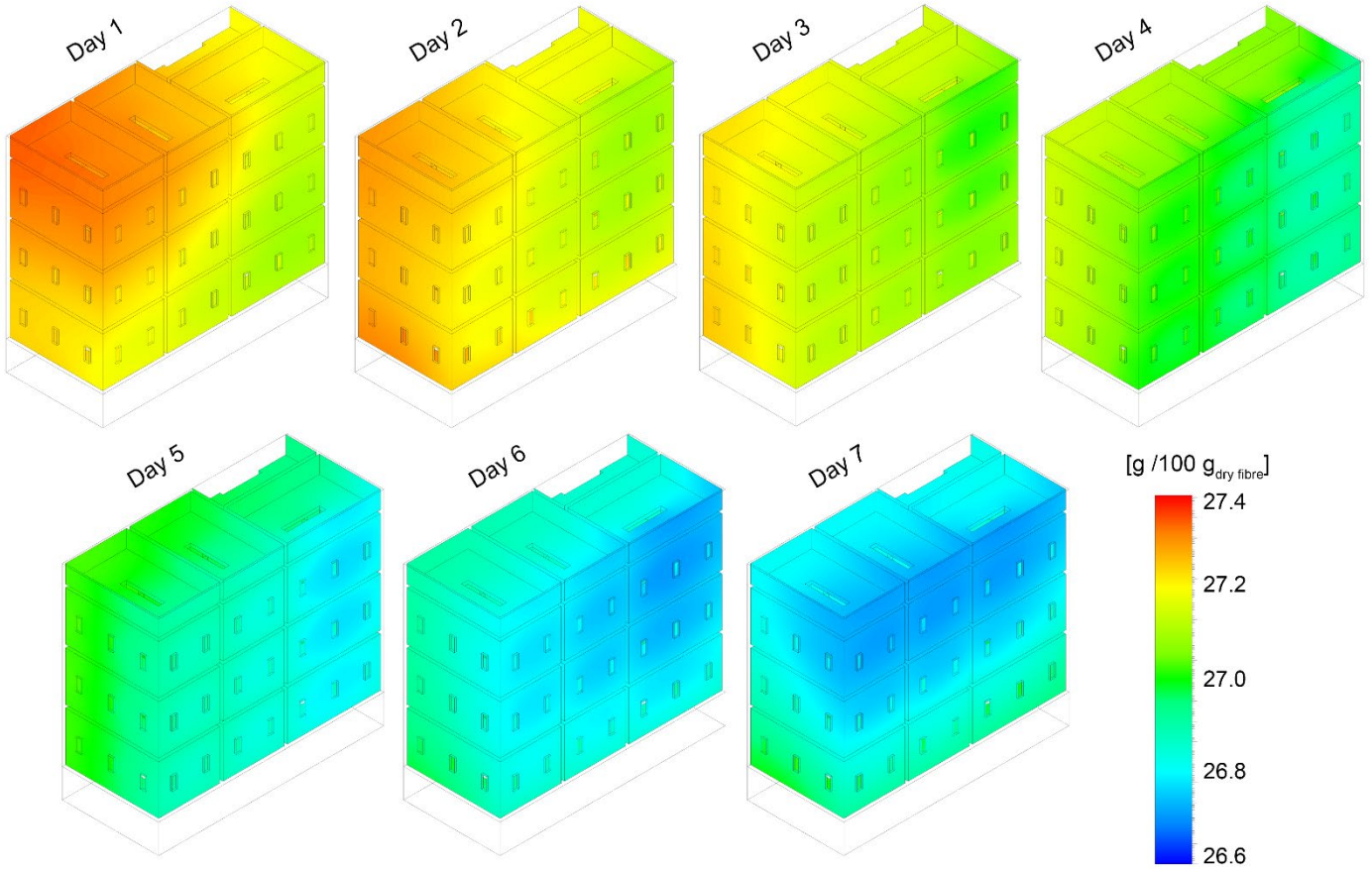

Figure 11: Simulated contours of carton moisture content profiles across carton surfaces for each day of the shipping period.

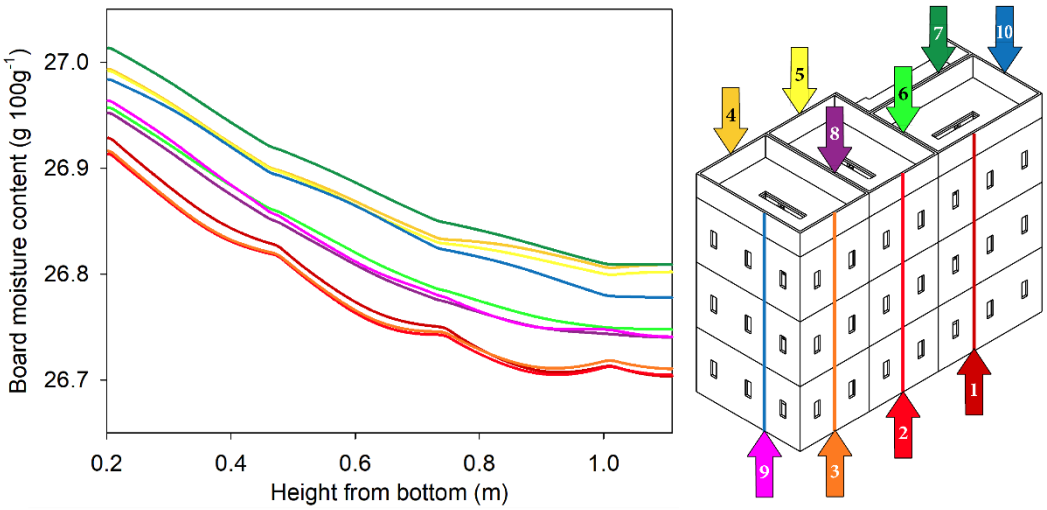

Figure 12: Moisture content along vertical lines through the corrugated fibreboard cartons showing moisture gradients on day 7. Colour coded arrows are correlated to the graph line colours.

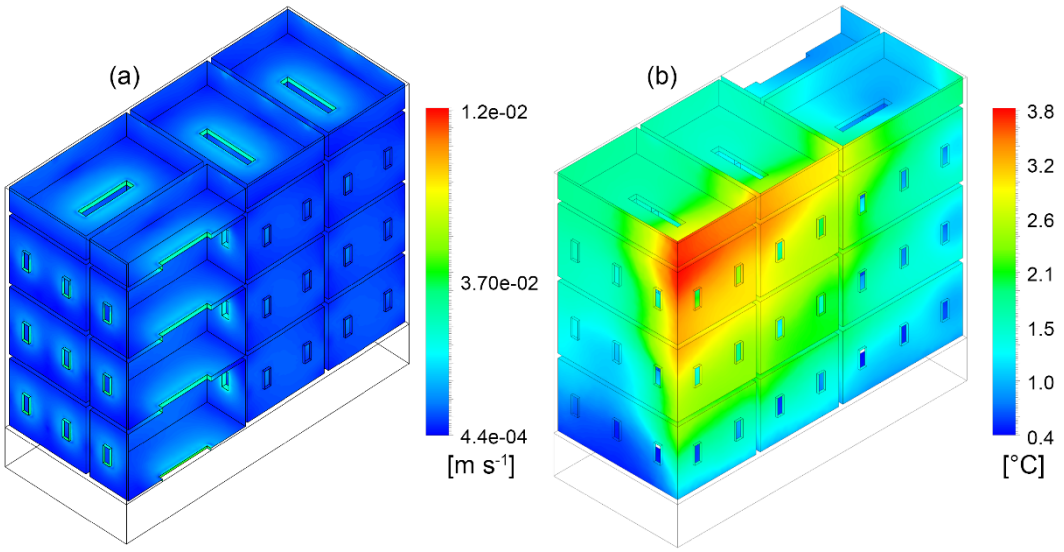

Figure 13: Simulated contours of (a) convective mass transfer coefficient profile across carton surfaces and (b) the temperature profile on day 7.